ELSEVIER

Journal of Hydrology 206 (1998) 191–218

Journal of Hydrology

Processes controlling colloid composition in a fractured and karstic aquifer in eastern Tennessee, USA

John F. McCarthy[a,*], Lisa Shevenell[b]

[a]*Environmental Sciences Division, Oak Ridge National Laboratory, P.O. Box 2008, Bethel Valley Road, Oak Ridge, TN 37831-6036, USA*
[b]*Nevada Bureau of Mines and Geology, MS 178 University of Nevada, Reno, NV, USA*

Received 24 February 1997; revised 11 December 1997; accepted 8 January 1998

Abstract

Groundwater was sampled from a number of wells along recharge pathways between fractured shale and karstic formations to evaluate the chemical and hydrologic mechanisms controlling the nature and abundance of groundwater colloids. The colloids recovered using low flow rate purging and sampling exhibited a composition and abundance consistent with lithology, flow paths, and effects of hydrology and aqueous chemistry on colloid mobilization and stability. In general, the larger-size colloids and Ca-containing colloids were more abundant in the karstic lithologies, while Na-containing colloids were more important in the shales. The composition of the colloids reflected recharge pathways from the fractured shale and dolomite formations on the ridges into the limestone in the valley floor. The Mg-colloids in the limestone reflect the possible contributions from the dolomite, while the Na, K, and Si reflect possible contributions from the shale. However, it was not possible to use the colloid composition as a signature to demonstrate colloid transport from one lithology to another. Mixing of recharge water from the shale with groundwater within the limestone formation and precipitation/dissolution reactions could account for the colloids present in the limestone without invoking transport of specific shale-derived colloids into the limestone formation. The abundance of colloids in groundwater appears to be controlled by both chemical factors affecting colloid stability, as well as physical factors related to hydrology (storm-driven recharge and water velocities). In general, colloids were more abundant in wells with low ionic strength, such as shallow wells in water table aquifers near sources of recharge at the top of the ridges. Increases in cation concentrations due to dissolution reactions along flow paths were associated with decreases in colloid abundance. However, in spite of elevated ionic strength, colloid concentrations tended to be unexpectedly high in karstic wells that were completed in cavities or water-bearing fractures. The higher levels of colloids appear to be related to storm-driven changes in chemistry or flow rates that causes resuspension of colloids settled within cavities and fractures. Published by Elsevier Science B.V.

Keywords: Colloids; Karst; Fractured; Colloid stability; Geochemical modeling

1. Introduction

The pathways and mechanisms of subsurface contaminant migration must be included in models of contaminant fate and transport if attempts to predict and remediate contaminant migration are to succeed. Models of contaminant transport processes typically treat aquifers as a two-phase system with contaminants partitioning between immobile solids and the mobile aqueous solution. However, components of the solid phase in the colloidal size range may also be mobile in subsurface environments and association of contaminants with mobile colloidal particles may,

* Corresponding author. Tel.: (423) 576-6606; fax (423) 576-3989; e-mail: mccarthyjf@ornl.gov

0022-1694/98/$19.00 Published by Elsevier Science B.V.
PII S0022-1694(98)00107-3

therefore, enhance the transport of sorbing pollutants (McDowell-Boyer et al., 1986; McCarthy and Zachara, 1989; McCarthy and Degueldre, 1993; Ryan and Elimelech, 1996).

Concerns about the potential role of colloids in contaminant transport are likely to be more significant in fractured formations than in unconsolidated porous media. Groundwater flow rates and colloid transport rates in fractured deposits are typically much higher than in granular deposits because most of the flow occurs in fractures, which constitute a relatively small portion of the total porosity of the aquifer. Colloids in fractured media can actually move faster than solutes because they are less strongly influenced by diffusion into micropores between fractures (matrix diffusion) which can greatly retard the transport of solutes (McKay et al., 1993). Furthermore, because of their relatively large size, colloids typically have diffusion coefficients ($\approx 10^{-11}$–10^{-13} m^2/s) that are 2–4 orders of magnitude smaller than solutes, and this will limit the opportunities for colloids to collide with immobile surfaces. Thus, over large distances and long time scales, colloids will tend to travel much further between collisions and, in general, have far fewer collisions—and opportunities to interact—with immobile surfaces than contaminant solutes. From a remediation perspective, it is also worth noting that colloids are restricted to the more transmissive zones of fractured systems. Thus, colloid-bound contaminants are more accessible for in-situ manipulations to immobilize the colloids or recover contaminants by pump-and-treat. As a result, strategies to utilize colloid manipulation to enhance remediation are likely to be more successful in fractured rather than granular formations.

In the present study, we focus on the US Department of Energy Oak Ridge Y-12 Plant which is located along a sequence of Cambrian fractured shales, and karstic limestones and dolomites in Eastern Tennessee (USA). Several hazardous and non-hazardous waste disposal sites are located in Bear Creek Valley and along Chestnut Ridge (Fig. 1) which have the potential for releasing various chemical constituents into local surface and ground waters. Previous work examined methods for sampling groundwater colloids in karst and fractured Bear Creek Valley formations (McCarthy and Shevenell, 1998). The objectives of the current study were to determine the nature and abundance of colloidal particles in groundwater across the range of lithologies present at the site and evaluate the geochemical and hydrologic processes controlling the abundance of colloids in a karst and fractured setting. The overall goal is to develop a conceptual model on the role of colloids at the Y-12 facility that would enable environmental managers to evaluate the importance of colloids to contaminant flux and to select appropriate remedial options.

2. Geologic setting

The study site is the Oak Ridge Y-12 Plant located in the Valley and Ridge physiographic province in the southern Appalachian fold and thrust belt. The study area is along Bear Creek Valley (Fig. 1) and the adjacent ridges which consist of Cambrian and Ordovician carbonate and clastic sedimentary rocks (King and Haase, 1987; Hatcher et al., 1992). These geologic units strike between N47° E to N67° E, with an average dip of 45° toward the southeast. The lower units evaluated in the current study are the Cambrian Nolichucky Shale and the Cambrian Pumpkin Valley Shale (Fig. 1). The Nolichucky Shale lies beneath Bear Creek Valley, is the site of most waste disposal areas at the plant, and is gradationally overlain by the Cambrian Maynardville Limestone. The Maynardville Limestone subcrops along the axis of Bear Creek Valley and is gradationally overlain by the Cambrian Copper Ridge Dolomite. The Maynardville Limestone and Copper Ridge Dolomite comprise the Knox Aquifer which is a karstic aquifer with numerous solution cavities and solutionally-enlarged fractures. Localized dissolution along fractures and bedding planes has increased both the matrix porosity and void space in the karstic parts of the Maynardville Limestone and Copper Ridge Dolomite (Goldstrand, 1995; Goldstrand and Shevenell, 1997). Up to 10.3% matrix porosity has been measured in the upper Maynardville Limestone (average of 2.1%, $n = 66$) whereas the lower Maynardville Limestone has lower porosity values of up to 2.3% (average of 0.5%, $n = 219$; Goldstrand and Shevenell, 1997).

Based on semiannual water level measurements in both conduit- and matrix-dominated portions of the aquifer and aquitards during static, non-storm,

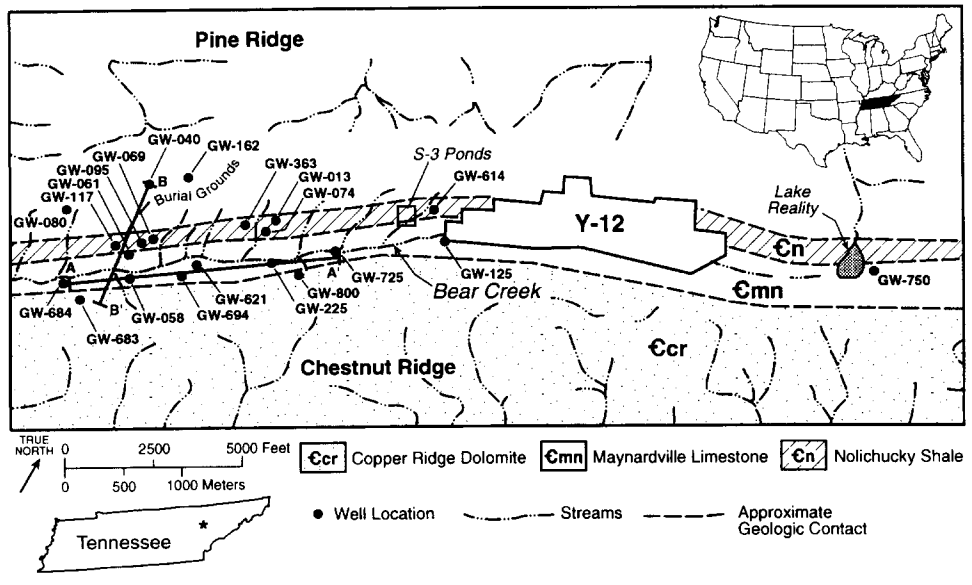

		Lithology	Thickness (m)		Formation	Permeability Types	Hydrologic Unit
CAMBRIAN	UPPER	Knox Group (OCk)	244 - 335	€cr	Copper Ridge Dolomite	Karstic: Conduit, Fracture, Matrix	Aquifer
		Conasauga Group (€c)	100 - 110	€mn	Maynardville Limetsone		
			150 - 180	€n	Nolichucky Shale	Fracture, Matrix	Aquitard
	MIDDLE		98 - 125	€dg	Dismal Gap Formation (Formerly Maryville Ls.)		
			25 - 34	€rg	Rogersville Shale		
			31 - 37	€f	Friendship Formation (Formerly Rutledge Ls.)		
	LOWER		56 - 70	€pv	Pumpkin Valley Shale		
			122 - 183	€r	Rome Formation		

Fig. 1. (a) Locations of wells sampled as part of this study at the Y-12 Plant. The approximate geologic contact between the Nolichucky Shale (aquitard) and the karstic Maynardville Limestone, and between the two karstic formations (Maynardville Limestone and Copper Ridge Dolomite) are illustrated with dashed lines. (b) A generalized stratigraphic column, including ages, is included.

conditions, recharge occurs locally along the adjacent ridges and flows toward the valley floor and the Maynardville Limestone. Locally, flow may not be strictly perpendicular to the equipotentials due to flow through anastomosing conduits, and this deviation from the general flow direction is recognized. Although absolute flow directions of individual packets of water in the conduit portions of the aquifer will vary from the general flow direction toward the valley floor due to the sinuous nature of the conduit passages (Shevenell and Beauchamp, 1994), water recharged on the ridges ultimately flows toward the valley

floor where flow becomes generally parallel to strike in the Maynardville Limestone. Abundant evidence exists for this general flow path. Clearly, water from the adjacent Nolichucky Shale aquitard flows toward the Maynardville Limestone, following the known hydrologic gradient, because many of the contaminants deposited in waste storage areas on the Nolichucky Shale have been measured in both conduit and matrix dominated wells in the Maynardville Limestone (e.g., HSW, 1993; Shevenell and Goldstrand, 1994).

Flow paths from the ridge formed by the Copper Ridge Dolomite to the Maynardville Limestone is less typical of porous media flow due to the extensive conduit development within both formations. General flow directions from the ridges to the valleys occurs, though likely not directly perpendicular to geologic strike as in the Nolichucky Shale due to the sinuous nature of the conduit passages. For instance, data from one location in the Copper Ridge Dolomite-Maynardville Limestone (Shevenell et al., 1992; Desmarais, 1995) show direct conduit and fracture connections between the two wells (GW-683, GW-684) and a downgradient spring which is located in the valley floor in the Maynardville Limestone $\approx$ 120 m away from the more distant well (GW-683). During drilling of the two wells, increased turbidity was observed in the spring (Shevenell et al., 1994). Also the two wells and the spring respond nearly identically to storm events (Desmarais, 1995). Injection tests in GW-684 resulted in distinct water level responses in both GW-683 and the spring (Shevenell et al., 1995). These data reveal that there is a conduit or fracture connection between GW-683 in the Copper Ridge Dolomite and GW-684 and the spring in the Maynardville Limestone. Both GW-684 and the spring have lower piezometric heads than the Copper Ridge Dolomite well (Desmarais, 1995; unpublished water level data; Shevenell and McMaster, 1996), indicating that there is downgradient flow from the Copper Ridge Dolomite to the Maynardville Limestone at this location, and presumably others.

There is also evidence that matrix and fracture flow transmit waters from the Nolichucky Shale to the Maynardville Limestone. Few traditional dye tracer tests have been conducted at the study site, and most have had their reliability called into question. In lieu of such information, previous workers have noted the presence and types of contaminants in the Maynardville Limestone through time (e.g. HSW, 1993). For instance, nitrate contamination, which could only have originated from the S-3 ponds site (located on the Nolichucky Shale) at the west edge of the Y-12 Plant (Fig. 1), has been detected in both conduit (e.g. GW-621, 1992 concentrations of 7 mg/l) and non-conduit wells (e.g. GW-061 and GW-225, 1992 concentrations of 27 and 75 mg/l, respectively) over 2100 m down gradient to the west (HSW, 1993; Shevenell et al., 1994). Nitrate is observed in both conduit and non-conduit wells throughout the distance between the S-3 ponds site and the downgradient GW-621 well site area. This nitrate tracer clearly demonstrates that flow from the Nolichucky Shale to the Maynardville Limestone occurs, and that flow in the Maynardville Limestone is along strike through the valley floor. Similar arguments could be made for other contaminants from the S-3 ponds site to downgradient locations in the Maynardville Limestone. The conduit, fracture and matrix portions of the aquifer all contribute to the observed contaminant distribution (Shevenell et al., 1994)

The Maynardville Limestone appears to act as a hydraulic drain for Bear Creek Valley. To the east of the S-3 Ponds site (Fig. 1), surface and groundwater flow is toward the east into the drainage of Upper East Fork Poplar Creek, whereas west of this site, flow is toward the west through the Maynardville Limestone.

Conduit flow in the Maynardville Limestone is generally at elevations between 180 and 290 m and is dominantly strike parallel through partially to totally mud-filled conduits with vertical dimensions of up to 12 m, but typically less than 1.5 m. Recognized conduit flow in the Copper Ridge Dolomite is generally above 290 m in elevation, with flow both parallel and perpendicular to the geologic strike through conduits which tend to be larger than those in the Maynardville Limestone, yet are often not fully saturated at the shallower depths. Although it has typically been reported in karst studies that conduits are difficult to intercept through drilling, a large percentage (66%) of wells drilled in carbonate units (Maynardville Limestone and Copper Ridge Dolomite) at the study site have encountered at least one cavity indicating that cavities are pervasive throughout the site (Shevenell and Beauchamp, 1994). Because so many wells have

Table 1
Summary of well construction and completion zones

Well	Lithology	Well elevation (m)	Date	Casing material	Screen material	Casing diameter (cm)	Completion interval (m)	Sampling depth (m)	Water level (m)	Rapid reponse	Aquifer
GW-683	Ccr	295.6	Dec-90	SS/#304	SS/sw/.01	11.4	44.5–60.0	51.8	27.0	Yes	K/WBF
GW-800	Ccr	293.1	Apr-93	SS/#304	SS/sw/.01	11.4	6.1–9.1	7.0	5.9	Likely	WT-K
GW-058	Cmn	277.3	Mar-84	SS/#304	SS/sw/.01	6.0	12.8–13.5	13.1	7.6	Likely	K/F
GW-061	Cmn	274.6	Mar-84	SS/#304	SS/sw/.01	6.0	6.1–7.5	6.7	5.1	Likely	WT-K
GW-095	Cmn	276.8	Sep-84	SS/#304	SS/sw/.01	11.4	41.1–47.5	43.6	2.8	?	K/F
GW-225	Cmn	286.6	Oct-85	Steel	OPEN	11.4	45.7–61.0	53.4	4.0	Yes	K/F
GW-226	Cmn	286.8	Oct-85	Steel	OPEN	11.4	13.7–16.8	14.3	6.0	Moderately	K/F
GW-621	Cmn	281.4	Sep-89	SS/#304	SS/sw/.01	11.4	7.6–12.3	12.0	6.8	Yes	WT-K/C
GW-684	Cmn	273.0	Oct-90	SS/#304	SS/sw/.01	11.4	34.8–39.1	36.6	4.7	Yes	K/F/C
GW-694	Cmn	286.2	Feb-91	Steel/F25	OPEN	17.8	47.0–62.3	53.4	7.6	Yes	K/F/C
GW-725	Cmn	292.2	Aug-91	Steel	OPEN	17.8	40.4–43.4	42.1	3.6	Moderately	K/WBF
GW-750	Cmn/Cn	279.3	Feb-92	SS/#304	SS/sw/.01	11.4	18.9–22.1	21.3	3.4	Moderately	K/F
GW-013	Cn	293.4	Sep-83	SS/#304	SS/sw/.01	6.0	2.6–3.2	2.9	2.0	Likely	WT-A
GW-069	Cn	281.8	Mar-84	SS/#304	SS/sw/.01	6.0	27.1–30.2	28.7	3.2	Not likely	A
GW-074	Cn	291.6	Mar-84	SS/#304	SS/sw/.01	6.0	56.4–62.8	59.1	artesian	Not likely	A
GW-117	Cn	277.8	Jun-85	Steel/F25	OPEN	11.4	146.3–161	155.5	0.1	Not likely	A
GW-125	Cn	306.1	Jul-85	Steel/F25	OPEN	11.4	153.0–168	153.4	1.5	Not likely	A
GW-363	Cn	291.3	Mar-88	Steel/F25	OPEN	16.8	15.2–22.9	19.1	2.1	Not likely	A
GW-614	Cn	307.7	Jul-89	SS/#304	SS/sw/.01	11.4	22.9–27.5	24.4	2.4	Not likely	A
GW-040	Cpv	306.1	Sep-83	SS/#304	SS/sw/.01	6.0	7.9–8.4	8.5	7.2	Likely	WT-A
GW-162	Cpv	316.5	Nov-85	Steel/F25	OPEN	16.8	28.1–38.1	33.5	7.2	Not likely	A
GW-080	Cr	297.9	Mar-84	SS/#304	SS/sw/.01	6.0	7.6–9.1	8.3	6.9	Likely	WT-A

Note: Well completion data are summarized from Jones et al. (1992). Ccr = Copper Ridge Dolomite, Cmn = Maynardville Limestone, Cn = Nolichucky Shale, Cpv = Pumpkin Valley Shale, Cr = Rogersville Shale, SS = stainless steel, sw/.01 = spiral wound screen with 0.01-in. opening, WT-A = water table well in an aquitard, WT-K = water table well in the karst aquifer, K/F = karst or fractured aquifer below the water table, K/WBF = karst with water-bearing fracture, C = competed in a cavity, and A = aquitard below the water table.

intercepted cavities at the study site, sampling and testing of the aquifer wells in this and previous studies have included both the turbulent flow regime represented by the conduits, as well as the more diffuse, laminar flow regimes represented by the matrix-dominated flow.

3. Methods

3.1. Selection of wells for sample collection

Twenty-one wells were sampled using low-flow sampling techniques to identify the nature and abundance of colloidal material in groundwater. Characteristics of the wells are shown in Table 1. Wells were selected such that at least two were completed within each of the three major geologic units so that variations between lithologies could be evaluated—shales (Nolichucky, Rogersville and Pumpkin Valley Shale), limestone (Maynardville Limestone) and dolomite (Copper Ridge Dolomite). In addition, within each non-carbonate unit, both shallow (<15 m) and deeper (>50 m) wells were selected such that comparisons could be made between younger, more rapidly flowing waters, and deeper, older waters. Within the two karstic units, sites known to encounter rapid flow through conduits, as well as sites experiencing slower flow through less transmissive zones, were also selected to test the hypothesis that higher colloid contents or size fractions may be associated with the larger karstic features. The potentially higher fluid velocities that would typically occur in the fractured portions of the shales and portions of the karstic units

Table 2
Water chemistry in unfiltered ground water: water quality parameters and concentration of major anions

Well no.	Temp (°C)	pH	Redox (mV)	Conductance (mS/cm)	DO (mg/l)	TSS (mg/l)	HCO3 (mg/l)	Cl (mg/)	F (mg/l)	NO3 (mg/l)	SO4 (mg/l)	TOC (mg/l)
GW-683	17.6	7.33	241.7	0.5	3.0	6.0	228.14	14.0	0.2	41.0	21.0	0.79
GW-800	14.8	7.06	215.5	0.43	4.0	1.0	264.7	2.0	0.1	0.2	10.0	1.27
GW-058	21.5	7.05	157.3	0.66	4.0	1.0	N/A	21.0	0.1	2.3	25.0	1.56
GW-061	17.9	7.05	258	0.68	1.17	N/A	228.1	19.0	0.17	80.0	30.0	0.77
GW-095	18.5	9.29	−118.7	0.52	0.88	N/A	348.9	2.0	0.57	1.0	9.6	0.45
GW-225	16.6	7.39	38.3	0.91	0.9	2.0	255.0	43.0	0.6	0.8	38.0	0.55
GW-621	22.1	7.68	167.5	0.32	4.0	5.0	N/A	3.7	0.1	5.1	7.5	0.25
GW-684	12.9	7.59	179.7	0.72	1.11	3.0	258.6	23.0	0.5	1.1	23.0	1.50
GW-694	12.2	7.41	155.3	0.56	1.11	1.0	284.3	17.0	0.3	2.8	17.0	0.90
GW-725	14.1	6.75	148.7	1.16	0.83	1.0	394.1	53.0	0.2	1.25	40.0	1.23
GW-750	17.1	7.41	110.3	0.49	0.82	1.0	290.4	5.0	0.1	0.1	18.0	1.13
GW-013	23.2	6.49	20.3	0.6	3.0	1.0	374.5	4.0	0.1	1.3	3.7	1.64
GW-069	30.7	8.20	−290	0.46	0.71	N/A	165.9	45.0	0.11	1.0	2.5	0.57
GW-074	27.2	9.40	−318	0.73	0.69	N/A	400.2	1.7	0.39	1.0	6.0	0.21
GW-117	25.1	9.06	27.7	3.34	1.0	7.0	N/A	670	4.0	0.1	25.0	1.50
GW-125	26.2	9.63	−130.5	2.72	0.72	N/A	1074.8	160	6.3	1.0	57.0	2.93
GW-363	20.5	8.95	192.3	0.44	0.58	N/A	237.9	1.8	0.24	1.0	7.2	0.21
GW-614-93	12.4	7.66	141.7	0.34	1.01	< 1.0	207.4	1.0	0.1	0.1	11.0	0.37
GW-614-95	N/A	7.31	206	0.34	0.85	N/A	205.0	1.7	N/A	1.0	11.0	0.06
GW-040	19.5	6.03	159.3	0.16	1.95	N/A	43.9	2.2	0.44	1.0	31.0	0.72
GW-162	21.9	7.49	200	0.29	0.36	N/A	137.9	3.4	0.14	1.0	8.9	0.3
GW-080	11.4	6.04	201	0.09	1.5	N/A	37.8	1.6	0.1	1.0	12.0	N/A

N/A = not analyzed.

Table 3
Water chemistry in unfiltered ground water: concentrations of major cations (mg/l)

Well no.	Al	Ba	B	Ca	Fe	Mg	Mn	Ni	K	Na	Sr	Si
GW-683	0.12	0.13	0.11	68.0	0.22	21.0	0.013	0.023	2.0	8.7	0.15	N/A
GW-800	0.02[d]	0.12	0.025	54.0	0.005[d]	22.0	0.001[d]	0.01[d]	2.5	0.88	0.11	N/A
GW-058	0.02[d]	0.08	0.063	85.0	0.005[d]	28.0	0.006	0.01[d]	1.7	13.0	0.12	N/A
GW-061	0.04[d]	0.078	0.082	93.0	0.01[d]	16.0	0.002[d]	0.02[d]	3.7	12.0	0.19	4.2
GW-095	0.04[d]	0.022	1.0	1.1	0.01[d]	0.35	0.002[d]	0.02[d]	3.2	140	0.089	4.5
GW-225	0.022[d]	0.12	0.079	83.0	0.33	41.0	0.052	0.011[d]	3.0	16.0	1.5	3.6
GW-621	0.33	0.02	0.0098	53.0	0.52	10.0	0.019	0.04	0.95	1.6	0.056	N/A
GW-684	0.54	0.11	0.077	66.0	0.24	16.0	0.082	0.009[d]	4.0	15.0	0.18	5.0
GW-694	0.039	0.099	0.048	78.0	0.41	17.0	0.23	0.011[d]	2.3	9.5	0.18	3.3
GW-725	0.05	0.19	0.039[c]	130	0.39	19.0	0.55	0.009[d]	2.6	19.0	0.31	3.3
GW-750	0.069	0.63	0.088	60.0	0.21	9.4	0.036	0.009[d]	4.1	4.6	0.71	6.9
GW-013	0.025	0.53	0.011	110	1.5	14.0	1.2	0.01[d]	2.0	4.1	0.21	N/A
GW-069	0.052	0.4	0.094	12.0	0.034	6.0	0.0019	0.01	4.3	61.0	0.98	6.7
GW-074	0.043	0.03	0.32	0.9	0.0058	0.19	0.001[d]	0.01[d]	2.0	140	0.052	4.9
GW-117	0.19	0.12	0.39	2.5	2.5	0.89	0.023	0.01[d]	8.0	710	0.35	N/A
GW-125	0.02[d]	0.07	0.67	1.2	0.23	0.78	0.005	0.01[d]	9.8	540	0.24	0.9
GW-363	0.1	0.072	0.32	2.7	0.2	1.2	0.002[d]	0.02[d]	2.0	110	0.1	4.7
GW-614-93	0.02[d]	0.16	0.018	47.0	0.062	10.0	0.02	0.01[d]	1.7	11.0	0.61	N/A
GW-614-95	0.043	0.14	0.013	41.0	0.045	7.9	0.024	0.01[d]	1.3	11.0	0.49	9.5
GW-040	3.7	0.094	0.017	6.6	5.8	8.2	1.2	0.01[d]	3.2	13.0	0.019	21.0
GW-162	0.02[d]	0.27	0.041	31.0	0.23	5.3	0.12	0.01[d]	4.3	15.0	0.75	9.7
GW-080	0.37	0.022	0.021	3.8	0.47	4.2	0.064	0.013	2.4	8.0	0.016	9.6

[c]: possible contamination by lab; [d]: value was below detection levels; N/A = not analyzed.

subject to solutional enlargement was expected to result in greater colloidal transport. Given that most conduits are mud-filled, there appears to be a continuous source of small grain size particles which can be mobilized during periods of higher velocity flows. In addition, some wells were selected based on quarterly monitoring data which revealed elevated metals content in the total versus dissolved water samples, possibly indicative of the presence of colloids.

To evaluate the importance of aqueous chemistry on colloid stability and abundance, wells were also chosen to span a range of ionic strengths and compositions (calcium-type versus sodium-type waters) and pH (Tables 2 and 3). Note that all wells had been developed following well completion to clear the formation of drilling-induced turbidity. Each well is also purged routinely for compliance monitoring, and hence, any measured turbidity from these wells using low-flow pumping rates is believed to represent actual aquifer conditions rather than well completion artifacts.

3.2. Sampling colloids using low-flow minimal-drawdown purging and sampling

Colloidal constituents in groundwater were sampled using a low flow rate that did not stress the aquifer and create potential concerns about production of colloidal artifacts (USEPA, 1994; McCarthy and Shevenell, 1998). Wells were sampled using a variable speed peristaltic pump and 1/4-in. OD Tygon tubing. Wells were purged at a low flow rate (10–100 ml/min) until hydrologic and water quality parameters stabilized. Dissolved oxygen (DO) was measured using CheMetrics ampules with colorimetric analysis using a Hach DR2000 field portable spectrophotometer. Total organic carbon (TOC) was analyzed using a Shimadzu Model 5000 High Temperature Combustion TOC Analyzer. Samples for cation analysis were preserved using HNO_3 to pH < 2 and analyzed by inductively coupled plasma-atomic emission spectroscopy (ICP). Anions were measured using ion chromatography. Alkalinity was measured in the field immediately after sample collection by titration to pH 4.5. Turbidity was measured in the field immediately after collection using a Hach Ratio/XR turbidimeter.

3.3. Filtration

In addition to analysis of unfiltered samples, groundwater was filtered through different pore sizes of filters, including cross-flow filtration using polycarbonate membrane filters (Nucleopore) with nominal 0.45, 0.1 or 0.05 μm pore sizes, and tangential flow filtration using Amicon Hollow-Fiber or Spiral Filters with 3000 or 100 000 dalton molecular weight cut-offs. Globular proteins with molecular weights of 3000 or 100 000 daltons have diameters of $\approx$ 1 nm or 5 nm, respectively; these nominal diameters will be referred to in this manuscript to facilitate comparisons with the pore size descriptions for the membrane filters. All filtration was conducted on-line; that is, the groundwater sampling tube was attached to the inlet of the filters, and filtration occurred at the well-head without exposing the sample to the atmosphere. Filters in the filter assemblies were washed with Milli-Q water and then rinsed with $\approx$ 0.5–1 l of groundwater immediately prior to sample collection to equilibrate the surfaces of the filter assembly with solutes and colloids prior to sample collection. The tangential flow filter configuration, in which water flows along the surface of the filter, minimizes opportunities for colloids to block pores. Accumulation of a filter-cake on the 0.1- or 0.4-μm membrane filters was minimized by use of large diameter filters (142 mm) and small sample volumes (less than 3 l was passed through the filter, including the initial rinse that was discarded). Groundwater and colloids passing through the filters were analyzed for TOC and cation concentrations. All samples were preserved immediately after collection, stored on ice and analyzed within 48 h. Note that the composition of the colloids was calculated based on ICP analyses of the filtrates (not the filters); the amount and composition of colloids retained by a given filter was calculated as the difference between the unfiltered sample and the filtrate. Only unfiltered water was passed through each filter, rather than a cascade through a series of filters with decreasing pore sizes.

Several of the 0.1-μm polycarbonate filters were visualized by scanning electron microscopy using a Hitachi S-4500 Field Emission Gun Scanning Electron Microscope, and the elemental composition of the colloidal particles was determined by energy dispersive X-ray spectroscopy (EDX) using a Prinston

Table 4
Well data summary for 'large' colloids*

Formation	Well	Turbid	Al	Ba	Ca	Fe	Mg	K	Na	Si	TOC
Ccr	683	8.01	N/A	N/A	N/A	N/A	N/A	N/A	N/A	N/A	N/A
Ccr	800	0.044	i	0	0	0	0	0	0.03	N/A	0.244
									3.4%		19.2%
Cmn	58	0.641	i	0.002	1	i	i	i	0	N/A	0
				2.5%	1.2%						
Cmn	61**	0.504	0	i	0	i	0	1.4	0	0	0.038
								37.8%			5.0%
Cmn	95**	0.115	0	i	0	i	i	1	i	i	0.17
								31.3%			38.2%
Cmn	225	1.77	0	0	0	c	i	0.1	0	0.1	0
								3.3%		2.8%	
Cmn	621	9.99	0.303	0.003	3	0.485	0.1	0.1	i	N/A	0
			91.8%	15.0%	5.7%	93.3%	1.0%	10.5%			
Cmn	684	3.77	0.517	0.022	8	c	1	0.8	3	1.6	0.159
			95.7%	20.0%	12.1%		6.3%	20.0%	20.0%	32.0%	10.6%
Cmn	694	4.52	0.017[d]	0	i	0.404[d]	i	0.1	i	0	0
			43.6%			98.6%		4.3%			
Cmn	725	4.96	i	0.04	30	c	5	0.7	4	0.7	0.474
				21.1%	23.1%		26.3%	26.9%	21.1%	21.2%	38.5%
Cmn/Cn	750	0.195	0.047	0.05	5	c	0.7	0.3	0.2	0.5	0
			68.1%	7.9%	8.3%		7.4%	7.3%	4.3%	7.2%	
Cn	13	1.5	0.005[d]	0	0	0.3	1	0.8	i	N/A	0.049
			20.0%			20.0%	7.1%	40.0%			3.0%
Cn	69	0.124	i	i	i	0.018	i	i	i	i	0.071
						52.9%					12.5%
Cn	74	0.431	i	0.003	i	i	i	1.33	0	i	c
				10.0%				66.5%			
Cn	117	10.95	0.17[d]	0.02	0.4	2.488	0.06	0	0	N/A	0
			89.5%	16.7%	16.0%	99.5%	6.7%				
Cn	125**	2.78	i	0.006	0.1	0.216	0.02	0.2	10	0.04	0.831
				8.6%	8.3%	93.9%	2.6%	2.0%	1.9%	4.4%	28.4%
Cn	363**	1.015	0.06[d]	0.5	0.2	0.05	0	0.4	0	0	0.002
			60.0%	6.9%	7.4%	25.0%		20.0%			1.0%
Cn	614—1993	0.222	i	0	0	0.003	i	i	0	N/A	0.022
						4.8%					6.0%
Cn	614—1995	0.102	i	i	i	0.04[d]	i	i	0	i	0
						88.9%					
Cpv	40**	224	3.659	0.051	0.2	4.5	0.8	1.4	0	5	0.305
			98.9%	54.3%	3.0%	77.6%	9.8%	43.8%		23.8%	42.2%
Cpv	162**	1.394	i	0	0	0.225[d]	0	1.2	0	0.1	0.104
						97.8%		27.9%		1.0%	34.7%
Cr	80***	9.97	0.331	0.001	i	0.452	0.1	i	0.1	0.4	N/A
			89.5%	4.6%		96.2%	2.4%		1.3%	4.2%	

*Concentration (mg/l) and percentage of total in size range >0.1 μm or 0.4 μm, where percentage calculations were determined as [(Unfiltered − (<0.1 μm or <0.4 μm))/Unfiltered × 100%].

**Indicates 0.4 -μm membrane filter was used instead of 0.1-μm. ***Reported filtrate for GW-080 was 0.05 μm.

c: possible contamination by lab; [d]: value was below detection limit; i: inconclusive data.

Note that B, Mn, Ni and Sr were measured, but were not present at significant concentrations.

Table 5
Well data summary for 'small' colloids*

Formation	Well	Turbidity	Al	Ba	Ca	Fe	Mg	K	Na	Si	TOC
Ccr	683	8.01	N/A	N/A	N/A	N/A	N/A	N/A	N/A	N/A	N/A
Ccr	800	0.044	i	0	0	0	0	0.1	0.02	N/A	0.117
								4.0%	2.3%		9.2%
Cmn	58	0.641	0.003	0	1	i	1	i	0	N/A	0
			15.0%		1.2%		3.6%				
Cmn	61**	0.504	0	0.007	0	0.009[d]	0	i	0	0	0.01
				9.0%		90.0%					1.3%
Cmn	95**	0.115	0	0.004	0.1	i	0.03	i	10	0.3	0
				18.2%	9.1%		8.6%		7.1%	6.7%	
Cmn	225	1.77	0	0	i	c	i	0.1	i	i	0.537
								3.3%			97.3%
Cmn	621	9.99	0.007	0	0	0.027	i	0.13	0	N/A	0
			2.1%			5.2%		13.7%			
Cmn	684	3.77	i	0.004	2	0.0018	1	0.1	1	0.2	0.142
				3.6%	3.0%	0.8%	6.3%	2.5%	6.7%	4.0%	9.5%
Cmn	694	4.52	i	0.003	2	i	1	0.1	0.2	0.1	0.708
				3.0%	2.6%		5.9%	4.3%	2.1%	3.0%	78.8%
Cmn	725	4.96	0.027	0.02	6	c	1	0.1	2	0.3	0
			54.0%	10.5%	4.6%		5.3%	3.8%	10.5%	9.1%	
Cmn/Cn	750	0.195	i	i	i	c	i	i	i	i	0
Cn	13	1.5	i	0.01	10	0.1	0	i	0	N/A	0
				1.9%	9.1%	6.7%					
Cn	69	0.124	0.058	0.05	2	0.009	0.7	0.4	6	0.7	0.033
			111.5%	12.5%	16.7%	27.1%	11.7%	9.3%	9.8%	10.4%	5.8%
Cn	74	0.431	0.006	0.005	i	i	0	i	i	0	c
			14.0%	16.7%							
Cn	117	10.95	0	0	0.1	0.0025	0.03	0.2	30	N/A	0.393
					4.0%	0.1%	3.4%	2.5%	4.2%		26.1%
Cn	125**	2.78	0.039[d]	i	0	0.0059	0	i	i	i	0.002
			195.0%			2.6%					0.1%
Cn	363**	1.015	i	i	i	0.136	0	i	0	0	0.083
							68.0%				40.1%
Cn	614—1993	0.222	0.019	0.01	2	0.001	1	0.2	1	N/A	0.1
			95.0%	6.2%	4.3%	1.6%	10.0%	11.8%	9.1%		27.2%
Cn	614—1995	0.102	0.021	0.01	2	0	0.4	0.1	0	0.5	0
			48.8%	7.1%	4.9%		5.1%	7.7%		5.3%	
Cpv	40**	224	0.002	0.004	0.2	0.2	0.1	1.2[d]	0	0	0.117
			0.1%	4.3%	3.0%	3.4%	1.2%	37.5%			16.2%
Cpv	162**	1.394	0.017[d]	0	1	0	0.1	i	0	0.1	0.041
			85.0%		3.2%		1.9%			1.0%	13.6%
Cr	80	9.97	N/A	N/A	N/A	N/A	N/A	N/A	N/A	N/A	N/A

*Concentration (mg/l) and percentage of total in size range between 0.1 and 0.4 μm and 1–5 nm, where percentage calculations determined by [(<0.1 μm − < 1 nm)/Unfiltered × 100%].

**Indicates 0.4 μm membrane filter was used instead of 0.1 μm.

c: possible contamination by lab; [d]: value was below detection limits; i: inconclusive data.

Note that B, Mn, Ni and Sr were measured, but were not present at significant concentrations.

Table 6
Well data summary for all colloids*

Formation	Well	Turbidity	Al	Ba	Ca	Fe	Mg	K	Na	Si	TOC
Ccr	683	8.01	0.095	0.01	4	0.215[d]	0	0	0.6	N/A	N/A
			79.2%	7.7%	5.9%	97.7%			6.9%		
Ccr	800	0.044	i	0	0	0	0	0.1	0.05	N/A	0.361
								4.0%	5.7%		28.4%
Cmn	58	0.641	0	0.002	2	i	0	i	0	N/A	0
				2.5%	2.4%						
Cmn	61	0.504	0	0.006	0	0	0	1.2	0	0	0.048
				7.7%				32.4%			6.3%
Cmn	95	0.115	0	0.002	0.1	0	0.01	0.8	0	0.2	0.009
				9.1%	9.1%		2.9%	25.0%		4.4%	2.0%
Cmn	225	1.77	0	0	i	c	i	0.2	i	0	0.378
								6.7%			72.4%
Cmn	621	9.99	0.306	0.003	3	0.512	0	0.23	i	N/A	0
			92.7%	15.0%	5.7%	98.5%		24.2%			
Cmn	684	3.77	0.508	0.026	10	0.2355[d]	2	0.9	4	1.8	0.301
			94.1%	23.6%	15.2%	98.1%	12.5%	22.5%	26.7%	36.0%	20.1%
Cmn	694	4.52	0.015	0.03	1	0.402	0	0.2	0	0.1	0.601
			38.5%	3.0%	1.3%	98.1%		8.7%		3.0%	66.9%
Cmn	725	4.96	0.026	0.06	36	c	6	0.8	6	1	0.146
			52.0%	31.6%	27.7%		31.6%	30.8%	31.6%	30.3%	11.9%
Cmn/Cn	750	0.195	0.041	0.01	2	c	0.2	0	0.1	0.1	0
			59.4%	1.6%	3.3%		2.1%		2.2%	1.4%	
Cn	13	1.5	0.004	0.01	10	0.4	1	0.5	i	N/A	0
			16.0%	1.9%	9.1%	26.7%	7.1%	25.0%			
Cn	69	0.124	i	0.03	1	0.027	0.3	0.1	4	0.4	0.104
				7.5%	8.3%	80.0%	5.0%	2.3%	6.6%	6.0%	18.3%
Cn	74	0.431	i	0.008	i	i	i	0.9	i	i	0.07
				26.7%				45.0%			33.0%
Cn	117	10.95	0.166	0.02	0.5	2.49	0.09	0.2	30	N/A	0.221
			87.4%	16.7%	20.0%	99.6%	10.1%	2.5%	4.2%		14.7%
Cn	125	2.78	0	0.005	0.1	0.22	0.02	i	i	0.02	0.833
				7.1%	8.3%	96.5%	2.6%			2.2%	28.5%
Cn	363	1.015	0.043	i	0.1	0.186	0	i	0	0	0.085
			43.0%		3.7%	93.0%					41.1%
Cn	614—1993	0.222	0	0.01	2	0.004	0	i	1	N/A	0.122
				6.2%	4.3%	6.5%			9.1%		33.2%
Cn	614—1995	0.102	0.013	0	0	0.029	0	0	0	0.1	0
			30.2%			64.4%				1.1%	
Cpv	40	224	3.661	0.055	0.4	4.7	0.9	2.6[d]	0	5	0.422
			98.9%	58.5%	6.1%	81.0%	11.0%	81.3%		23.8%	58.4%
Cpv	162	1.394	0	0	1	0.225[d]	0.1	0.6	0	0.2	0.145
					3.2%	97.8%	1.9%	14.0%		2.1%	48.5%
Cr	80	9.97	0.331	0.001	i	0.452	0.1	i	0.1	0.4	N/A
			89.5%	4.6%		96.25	2.4%		1.3%	4.2%	

*Concentration (mg/l) and percentage of total in size range >1–5 nm, where percentage calculations determined as [(Unfiltered – (<1 nm or <5 nm))/Unfiltered × 100%].

c: possible contamination by lab; [d]: value was below detection limits; i: inconclusive data.

Note that B, Mn, Ni and Sr were measured, but were not present at significant concentrations.

Gamma Tech Digital X-ray detector system. Filters were also analyzed for mineralogic composition using X-ray diffraction (XRD) using a Scintag XDS-2000.

3.4. Sampling during storm events

One well was sampled during storm events at closely spaced time intervals using a Model 3700 Isco automatic sampler with a Model 3230 Bubble Flow Meter. The sampling rate on the Isco was decreased to 200 ml/min by flow restriction using 1/4-in. Tygon tubing. One liter samples of groundwater were taken every $1\frac{1}{2}$ or 3 h. Sampling was initiated when the bubble flow meter detected a 3-in. rise in the water level elevation in the well following a storm event. Samples were returned to the laboratory and turbidity measured as above.

4. Results and discussion

4.1. Nature and abundance of colloids

Data on the composition and concentration of colloids are summarized in Tables 4–6, based on analysis of cations and TOC in unfiltered groundwater compared to similar analyses of filtrates. Many factors affect the retention of particles on filters and the difficulties in assigning specific dimensions to colloids based on filtration results have been discussed (Buffle, 1988; McCarthy and Degueldre, 1993). We feel that the most useful information provided by the filter separation is distinguishing generally between 'large' and 'small' colloids. Therefore, we define 'large' colloids (Table 4) as those retained by either a 0.1- or 0.45-μm filter (because of equipment or logistical problems, not all wells were sampled using the same size filters). 'Small' colloids are defined here as colloids that are not retained by the 0.1- or 0.45-μm filters, but that are retained by the 1- or 5-nm filter (Table 5). This encompasses a 100-fold difference between the small and large size cut. In addition, the total colloidal population (everything retained by the 1- or 5-nm filters), which encompasses both large and small colloids is presented in Table 6.

These tables list the measured mass concentrations of colloids, and the percentage of the individual constituents in the groundwater which is colloidal. For instance, the Fe in GW-117 accounts for nearly all of the mass in the colloidal phase (99.6%), whereas colloidal Ca constitutes only 20% of the Ca in the water (Table 6). Hence, in this sample, there is virtually no dissolved Fe, but a significant portion of the Ca is dissolved. In some instances, the data was judged to be 'inconclusive', generally indicating that the reported concentration of an analyte in a filtrate was slightly higher than in the unfiltered water or in a filtrate from a larger sized filter. In most cases, this situation occurred when the total concentration of the analyte was near the detection limit even in the unfiltered water or when there were small differences between two high concentrations (e.g. differences in Na in GW-117 or -125, Table 3). These inconclusive results reflect analytical uncertainty, but may also be related to changes in water chemistry over the course of sampling because the water was filtered on-line, and not pooled into a single batch that would average over any temporal variability prior to filtration. Nevertheless, clear patterns emerged in the nature and abundance of colloids that can be related to lithology, flow paths, and colloidal stability.

It should be noted that we report colloid concentrations with respect to the mass of colloidal cations (based on measurement of mg/l of elements in the colloidal phase). A given mass of colloids in the 'small' size range would represent a much larger number of colloidal particles and surface area of colloids than the same mass in the 'large' size range. The mass of colloids (C_m, mg colloids/l) is related to the number of particles (C_n, particles/l) as a function of particle density (ρ, which will be assumed to be 2.0 g/cm^3, taken as an average for clay, hydrated silica and iron hydroxide; McCarthy and Degueldre, 1993) and particle diameter (d):

$$C_m = C_n \frac{\pi \rho d^3}{6}$$

Thus, a colloid mass concentration of 0.1 mg/l is equivalent to $\approx 10^{11}$ particles/l of 0.1-μm diameter ('large') colloids, or 10^{15} particles/l of 5-nm diameter ('small') colloids. At this concentration, the total surface area of the 'small' colloids would be $\approx$ 20-fold greater than the equivalent mass of 'large' colloids. It

should also be noted that turbidity was not well correlated with the mass concentration of colloidal elements. This is not unexpected given the diversity of colloid sizes and composition. Large particles scatter light more effectively than small colloids, and colloids with a high refractive index, such as iron-oxides or clays, will likely have a greater effect on measured turbidity than similar concentrations of, for example, calcite colloids.

4.2. *Effects of lithology*

Colloids contain a range of cationic constituents consistent with the lithology of the parent formation. For example, most conduits in the Maynardville Limestone are partially or totally mud-filled. Shevenell (1994) reported that samples collected from mud filling one of the conduits (well GW-734) in the Maynardville Limestone contained significant concentrations of Ca (3100–25 000 μg/g). Mineralogic identification of the clays was not conducted. Small particles in the muds may be entrained in the waters resulting in significant colloidal Ca concentrations. Other elements found in high concentrations (in μg/g) in the muds in the cavity intersected by GW-734 are: Al = 6800–14 000, Fe = 16 000–34 000). The typically large amounts of colloidal Al, Fe, and Ca found in the Maynardville Limestone wells in this study are thus consistent with the fine-grained material in the muds (Tables 4–6). A typical calcite colloid from a Maynardville Limestone well is shown in Fig. 2(a).

The colloidal constituents of the shales are consistent with alteration products of the parent material. The mineralogical composition of the colloids was determined for selected wells analyzing material collected on 0.1-μm filters using XRD. The following mineral phases were identified:

GW-061: quartz, chlorite, minor mica, possible kaolinite;
GW-069: smectite;
GW-125: chlorite, possible clay (undetermined);
GW-162: possible chlorite and clay (undetermined), trace quartz;
GW-684: calcite, dolomite, trace quartz.

Although Ca-smectite has not been noted in mineralogic descriptions of the shales, Saunders and Toran (1994) postulate that the evolution of the $NaHCO_3$ waters in the shales are partially a result of weathering of K-illite and Na-feldspar to Ca-smectite, and the accompanying release of Na and Si as well as precipitation of $CaCO_3$. The XRD (above) and SEM/EDX (Fig. 2) analyses of the colloidal material on the filters is consistent with the presence of aluminosilicates with K and Fe substitution (e.g. shown in the EDX spectrum of the edge of a clay platelet for GW-040 in Fig. 2(b)), and smectite was identified as a colloid in GW-069. Iron oxide colloids are also present attached to the clay surfaces, as indicated by the higher Fe peaks on the EDX spectrum of the surface of a clay particle in GW-040 (Fig. 2(b)).

A significant fraction of the TOC in groundwater from most of the wells is also colloidal (Table 6, up to 72.4% in GW-225), indicating that most colloidal surfaces are organically coated. The organic coatings would be expected to adsorb to and reverse the surface charge of any positively charged surface, thus contributing to the colloidal stability of the particles.

The size distribution of the colloids is different in the carbonates and shales. The larger size fractions (>0.1 μm) tend to be more important in the wells monitoring karstic aquifers. All colloidal constituents for all wells within a particular unit are evaluated by noting if the majority (greater percentage and concentration) of colloids are in the larger or smaller size fractions. From this tally of all elements listed in Tables 4 and 5, 84% of the colloidal mass measured in the karstic Maynardville Limestone wells were in the larger (>0.1 μm) size fraction. In GW-684, for example, for all colloids measured, the concentrations in the large-size fraction are greater than those in the <0.1-μm size fraction (except Mg-colloids where equal concentrations of small and large colloids were identified). In contrast, there is an equal likelihood of small and large colloids occurring in the shale formations (50% of all measured colloids in all shale wells were in the small-size fraction).

Ca-containing colloids appear to be more important in the Maynardville Limestone than in the Nolichucky Shale. Higher Ca colloidal concentrations are observed in the >0.1-μm size fraction in the Maynardville Limestone in comparison to the Nolichucky Shale. This reflects the control of lithology and flow paths of the particular wells sampled. It is unlikely that any contributions from

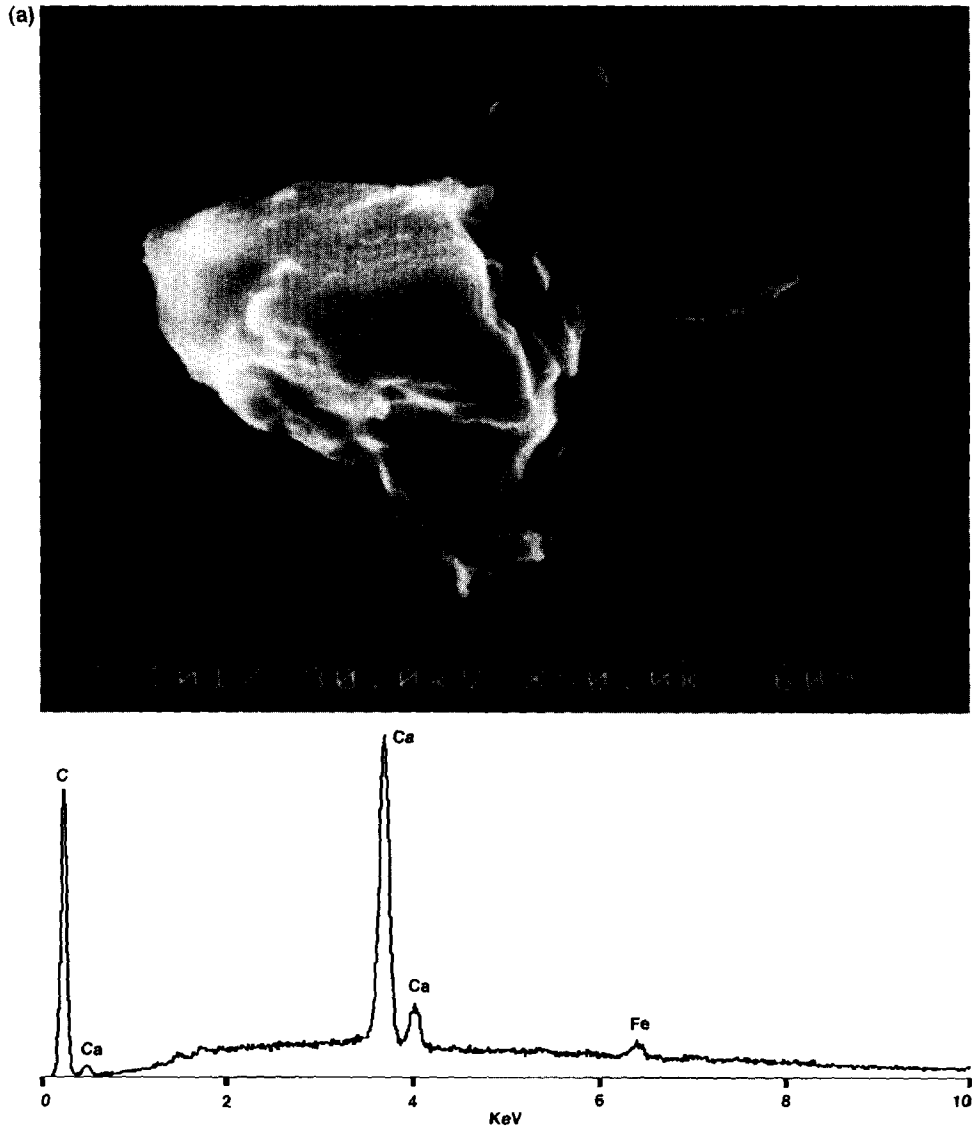

Fig. 2. SEM/EDX of colloidal particles from (a) well GW-095 in the Maynardville Limestone, and (b) GW-040 in the Pumpkin Valley Shale. The EDX spectra below the figures show the elemental composition of the colloids. In panel (a), the EDX focused on the surface of the colloid shown in white and demonstrated that the composition is dominated by calcium. In panel (b), the edge of the clay platelet (designated 'A') is composed of Al–Si with some K and Fe that may reflect subsititution within the aluminosilicate structure. The face of an adjacent clay platelet (designated 'B') contains a similar proportion of Al/Si/K (reflecting the composition of the aluminosilicate) with a much larger Fe component reflecting iron oxide coatings on the face of the colloid.

the Maynardville Limestone have entered the flow paths tapped by the Nolichucky Shale wells because water is recharged on Pine Ridge to the north, with flow in the Nolichucky Shale ultimately draining into the Maynardville Limestone (see Fig. 3). Hence, higher concentrations of Ca colloids are associated with the carbonates in the >0.1-μm size fraction, but they are considerably less important in the shales which have similar to higher Ca concentrations and percentages in the smaller size fractions. Hence,

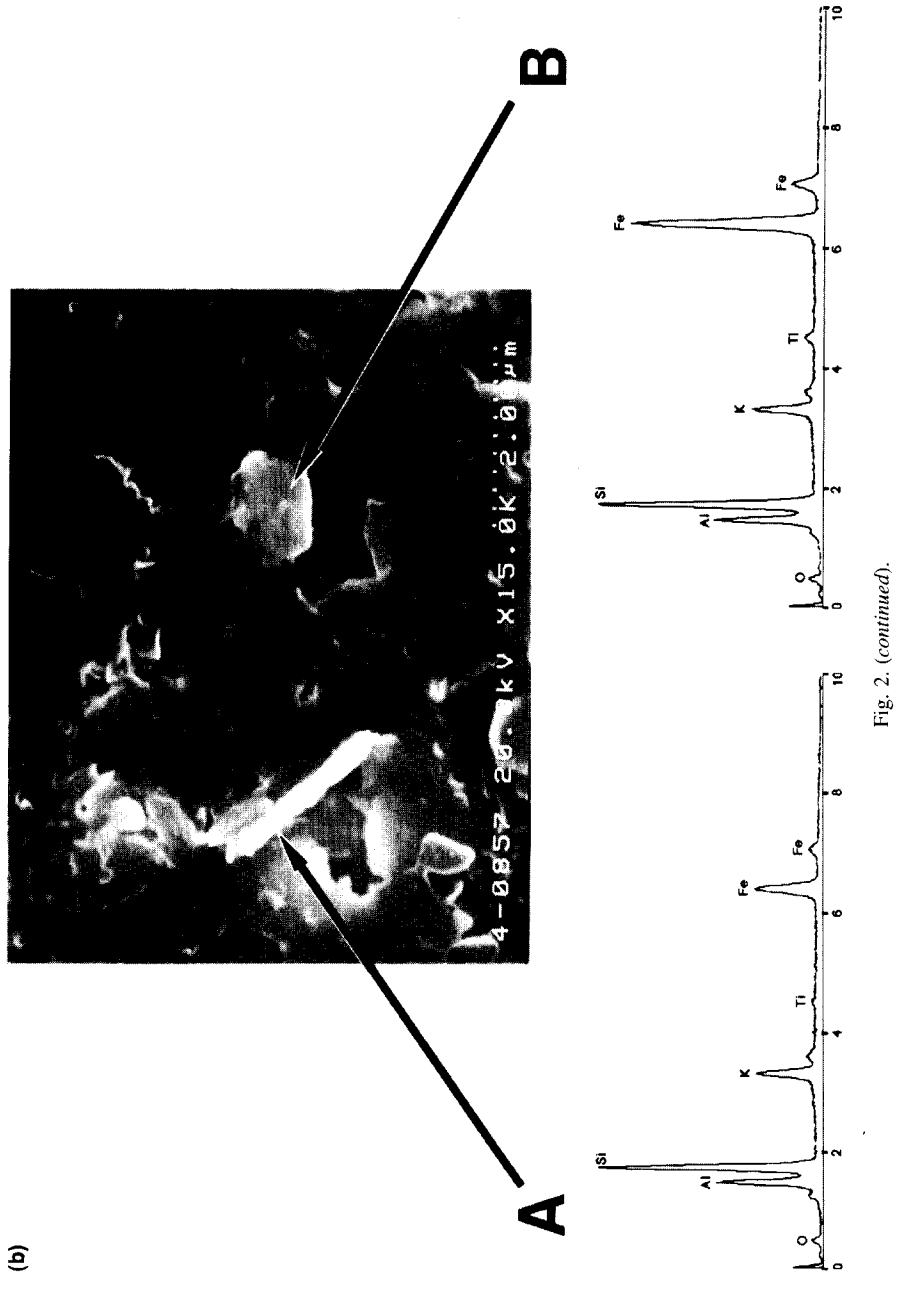

Fig. 2. (*continued*).

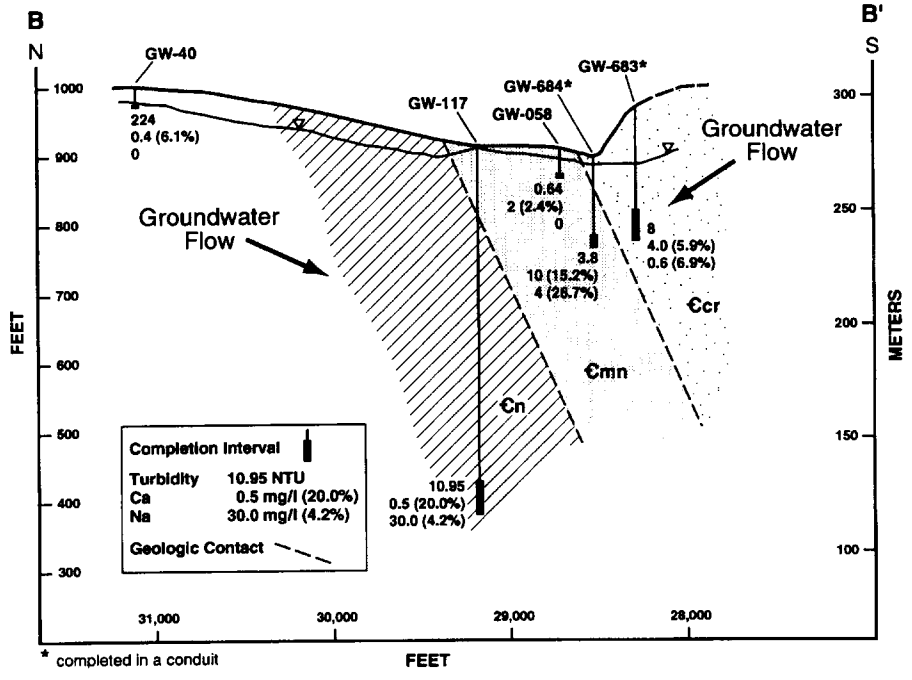

Fig. 3. Cross-section perpendicular to geologic strike showing measured turbidity, concentration and percentage total colloidal (all size fractions) Ca, and concentration and percentage colloidal Na for seven wells in this study. The location of this cross-section is noted in Fig. 1. Concentrations of Ca colloids are higher in the carbonates than in the Nolichucky Shale, yet form a smaller percentage of the total measured Ca in the fluid than in the Nolichucky Shale. Similarly, Na colloid concentrations are generally higher in the deeper portions of the Nolichucky Shale than in the carbonates, yet form a smaller percentage of the total measured Na in the fluid than in the carbonates.

lithology influences both the type and size of colloids, with smaller colloids being associated with the Nolichucky Shale, and larger ones being present in the Maynardville Limestone. This seems reasonable because the larger colloids could more easily move through the larger karstic features.

Absolute concentrations of Ca are lower in the Nolichucky Shale than in the Maynardville Limestone, but colloidal Ca may still constitute a significant portion of the total Ca in the Nolichucky Shale. For example, the Ca-colloid concentration in GW-117 is 0.4 mg/l in the >0.1-μm size fraction, which constitutes 16% of the Ca in this water (Table 6). In contrast, colloidal Na is more important in the shale wells than in the carbonate wells. Significant colloidal-Na (30 mg/l; 4.2% of the total Na) was detected in the smaller size fractions of well GW-117, whereas only 0.1 mg/l of Ca were measured in the smaller size fraction in this well, which constituted 4% of the Ca in the water (Table 5). The Na-colloid concentrations in the Maynardville Limestone in the larger size fractions are generally low (e.g. in GW-684, Na-colloids are 3 mg/l, or 20% of all Na in the water). Hence, although there are lower concentrations of colloidal Na (>0.1-μm size) in the Maynardville Limestone, they constitute a greater percentage of the total Na in the waters in the carbonate aquifer, which is generally lacking in Na-bearing minerals with which dissolution reactions could occur. Na in the Nolichucky Shale appears to predominantly occur in the smaller size fractions. The Na that does occur in the Maynardville Limestone wells is generally in the larger size fractions.

4.3. Geochemical modeling

The effect of the presence of colloids on typical geochemical modeling applications was examined using two sets of data: those collected in this study using low flow rate sampling protocols, and those

Table 7
Comparison of selected saturation indices for three well waters filtered through different filter sizes and collected during the current and previous work

	Barite	Calcite	Celestite	Dolomite	Gypsum
Saturation indices for GW-013					
Current work—turbidity = 0.07					
RAW	−0.242	−0.384	−3.990	−1.392	−2.728
0.1 μm	−0.242	−0.418	−3.979	−1.451	−2.759
1 nm	−0.241	−0.383	−3.989	−1.422	−2.727
Previous work—turbidity = 12					
RAW	−0.016	−0.815	−3.954	−2.288	−2.748
0.45 μm	−0.035	−0.818	−3.954	−2.327	−2.753
Saturation indices for GW-040					
Current work—turbidity = 224					
RAW	0.151	−2.963	−3.964	−5.553	−2.897
0.4 μm	−0.166	−2.958	−3.989	−5.575	−2.887
1 nm	−0.220	−2.970	−4.027	−5.590	−2.912
Previous work—turbidity = 1000					
RAW	0.669	−2.126	−3.764	−3.830	−2.953
0.45 μm	−0.176	−2.094	−3.979	−3.959	−2.867
Saturation indices for GW-800					
Current work—turbidity = 0.04					
RAW	−0.232	−0.369	−3.766	−0.877	−2.553
0.1 μm	−0.233	−0.369	−3.767	−0.878	−2.533
1 nm	−0.232	−0.369	−3.808	−0.878	−2.553
Previous work—turbidity = 66					
RAW	0.156	−0.023	−3.060	−0.118	−0.216
0.45 μm	0.118	−0.020	−3.072	−0.146	−2.152

collected during the compliance monitoring at high flow rates by the Y-12 Environmental Management Department, Ground Water Protection Program. The routine compliance monitoring utilized high flow rates and purging of three well volumes. Turbidity was observed to be up to two orders of magnitude greater in samples collected using the compliance monitoring sampling protocols compared to the low flow rate sampling employed in this study (McCarthy and Shevenell, 1998).

An equilibrium thermodynamic model (SOLMINEQ.88, Kharaka et al., 1988) was used to calculate saturation indices (SI) and compare the results between the different filtered size fractions. These results were used to determine how the presence of colloids and our assumptions about dissolved phases change interpretations of modeling results. The SI were evaluated for the minerals known to occur in each of the units, and these included anhydrite, barite, calcite, celestite, chlorite, clay, dolomite, glauconite, gypsum, hematite, illite, kaolinite, and pyrite (Saunders and Toran, 1994; Goldstrand, 1995; de Laguna et al., 1968).

Although mixing of waters may form additional minerals not noted here, we focus on the mineral phases actually known to be present in the different formations. Saturation indices were calculated for all waters collected during this study and some of these values are reported in Tables 7–9. Colloid abundance data from Tables 4–6 are compared with these SI results. SI for particular minerals often decrease in waters filtered through progressively smaller filters. For instance, 58.5% of the Ba in GW-040 is colloidal. When these colloids are removed through filtration, the SI of barite decreases from 0.151 to −0.22, reflecting this removal of colloidal Ba from the sample. As expected, other samples show similar trends for other minerals as well, although not always in a consistent

Table 8
Saturation indices in the dissolved (<1 nm) and raw water samples. These values are followed by the colloidal content of the elements which comprise the particular mineral

	Ccr—GW-080		Cmn—GW-061		Cmn—GW-095		Cmn—GW-684		Cmn—GW-694		Cmn—GW-725		Cmn/Cn—GW-750	
	< 0.05 μm	Unfiltered	< 1 nm	Unfiltered	< 1 nm	Unfiltered	< 100 K	Unfiltered	< 1 nm	Unfiltered	< 1 nm	Unfiltered	< 1 nm	Unfiltered
Barite	−0.657	−0.641	−0.094	−0.059	−1.116	−1.075	−0.032	0.108	−0.125	−0.061	0.362	0.465	0.641	0.693
Ba	0.01	4.6%	0.006	7.7%	0.002	9.1%	0.026	23.6%	0.03	3.0%	0.06	31.6%	0.01	1.6%
Calcite	−3.324	−3.338	−0.189	−0.189	0.243	0.284	0.134	0.193	0.109	0.113	−0.195	−0.197	0.098	0.110
Ca			0		0.1	9.1%	10	15.2%	1	1.3%	36	27.7%	2	3.3%
Celestite	−4.343	−4.348	−3.114	−3.114	−3.945	−3.920	−3.340	−3.208	−3.420	−3.344	−2.928	−2.824	−2.766	−2.708
Sr	0		0		0.005	5.6%	0.04	22.2%	0.01	5.6%	0.1	32.3%	0.02	2.8%
Dolomite	−6.403	−6.408	−0.878	−0.879	0.281	0.335	−0.104	0	−0.212	−0.211	−1.010	−0.990	−0.344	−0.326
Mg	0.1	2.4%	0		0.01	2.9%	2	12.5%	0		6	31.6%	0.2	2.1%
Gypsum	−3.450	−3.465	−1.891	−1.891	−4.285	−4.244	−2.212	−2.118	−2.420	−2.185	−1.772	−1.665	−2.310	−2.250
Ca			0		0.1	9.1%	10	15.2%	1	1.3%	36	27.7%	2	3.3%
FeO	**2.361**	**5.191**	−6.751	−6.751	−2.315	−2.315	−6.321	−4.603	**8.143**	**11.592**	−6.710	−6.028	−4.840	−4.725
Fe	0.452	96.2%	0		0		0.236	98.1%	0.402	98.1%				
Illite	2.962	6.392	5.226	5.327	1.948	2.091	4.320	8.468	4.960	5.338	4.408	4.989	5.810	6.488
K			1.2	32.4%	0.8	25.0%	0.9	22.5%	0.2	8.7%	0.8	30.8%	0	
Na	0.1	1.3%	0		0		4	26.7%	0		6	31.6%	0.1	2.2%
Al	0.331	89.5%	0		0		0.508	94.1%	0.015	38.5%	0.026	52.0%	0.041	59.4%
Si	0.4	4.2%	0		0.2	4.4%	1.8	36.0%	0.1	3.0%	1	30.3%	0.1	0.0%
Kaolinite	6.344	9.316	7.503	7.502	2.975	3.012	6.365	9.703	7.148	7.467	7.256	7.738	7.386	7.975
Al	0.331	89.5%	0		0		0.508	94.1%	0.015	38.5%	0.026	52.0%	0.041	59.4%
Si	0.4	4.2%	0		0.2	4.4%	1.8	36.0%	0.1	3.0%	1	30.3%	0.1	1.4%
Quartz	0.708	0.725	0.283	0.283	0.17	0.189	0.228	0.422	0.254	0.254	0.228	0.228	0.507	0.507
Si	0.4	4.2%	0		0.2	4.4%	1.8	36.0%	0.1	3.0%	1	30.3%	0.1	1.4%
Smectite	5.144	8.627	6.651	6.650	1.657	1.731	5.259	9.417	6.148	6.520	6.107	6.669	6.883	7.571
Ca			0		0.1	9.1%	10	15.2%	1	1.3%	36	27.7%	2	3.3%
Na	0.1	1.3%	0		0		4.000	26.7%	0		6	31.6%		
Al	0.331	89.5%	0		0		0.508	94.1%	0.015	38.5%	0.026	52.0%	0.041	59.4%
Si	0.4	4.2%	0		0.2	4.4%	1.8	36.0%	0.1	3.0%	1	30.3%	0.1	1.4%

Bold numbers in the FeO row are for hematite.

Table 9

Saturation indices in the dissolved (>1 nm) and raw water samples. The elemental composition of colloidal minerals is presented as in Table 8.

	Cn—GW-069		Cn—GW-125		Cn—GW-363		Cn—GW-614 (1995)		Cpv—GW-040		Cpv—GW-162	
	< 1 nm	Unfiltered	< 1 nm	Unfiltered	< 1 nm	Unfiltered	< 1 nm	Unfiltered	< 1 nm	Unfiltered	< 1 nm	Unfiltered
Barite	–0.577	–0.524	–0.305	–0.266	–0.37	–0.665	–0.022	–0.022	–0.22	0.151	0.009	0.019
Ba	0.03	7.5%	0.005	7.1%			0		0.055	58.5%	0	
Calcite	0.133	0.167	0.916	0.956	0.229	0.25	–0.355	–0.355	–2.97	–2.963	–0.32	–0.307
Ca	1	8.3%	0.1	8.3%	0.1	3.7%	0		0.4	6.1%	1	3.2%
Celestite	–3.422	–3.37	–3.144	–3.118	–3.958	–3.93	–3.020	–3.020	–4.027	–3.964	–2.936	–2.915
Sr	0.07	7.1%	0.01	4.2%	0.001	1.0%	0		0.003	15.8%	0.02	2.7%
Dolomite	0.264	0.317	1.918	1.97	0.402	0.423	–1.199	–1.199	–5.59	–5.553	–1.121	–1.102
Mg	0.3	5.0%	0.02	2.6%	0		0		0.9	11.0%	0.1	1.9%
Gypsum	–3.802	–3.744	–3.696	–3.651	–3.995	–3.949	–2.580	–2.580	–2.912	–2.897	–2.795	–2.771
Ca	1	8.3%	0.1	8.3%	0.1	3.7%	0		0.4	6.1%	1	3.2%
FeO	–3.854	–3.157	–1.691	–0.237	–2.669	–1.514	–6.333	–5.884	–6.588	–5.883	–5.87	–4.208
Fe	0.027	80.0%	0.22	96.5%	0.186	93.0%	0.029	64.4%	4.7	81.0%	0.225d	97.8%
Illite	3.554	3.475	–2.798	–2.799	2.972	3.455	6.517	6.891	1.724	9.91	4.982	5.059
K	0.1	2.3%					0		2.6d	81.3%	0.6	14.0%
Na	4	6.6%			0		0		0		0	
Al			0		0.043	43.0%	0.013	30.2%	3.661	98.9%	0	
Si	0.4	6.0%	0.02	2.2%	0		0.01	1.1%	5	23.8%	0.2	2.1%
Kaolinite	4.58	4.476	–1.04	–1.039	3.913	4.401	8.301	8.623	5.177	11.788	6.443	6.463
Al			0		0.043	43.0%	0.013	30.2%	3.661	98.9%	0	
Si	0.4	6.0%	0.02	2.2%	0		0.01	1.1%	5	23.8%	0.2	2.1%
Quartz	0.278	0.303	–0.786	–0.786	0.24	0.24	0.703	0.707	0.842	0.96	0.582	0.592
Si	0.4	6.0%	0.02	2.2%	0		0.01	1.1%	5	23.8%	0.2	2.1%
Smectite	3.784	3.702	–4.008	–4.001	2.852	3.424	8.027	8.407	4.211	12.072	5.992	6.033
Ca	1	8.3%	0.1	8.3%	0.1	3.7%	0		0.4	6.1%	1	3.2%
Na	4	6.6%			0		0		0		0	
Al	0.4	6.0%	0		0.043	43.0%	0.013	30.2%	3.661	98.9%	0	
Si			0.02	2.2%	0		0.01	1.1%	5	23.8%	0.2	2.1%

manner. When this trend is not observed, it is usually a result of the fact that the colloids occur in very low concentrations in the samples, and it cannot be verified with any confidence that an analysis at one size fraction is significantly different from that in another size fraction.

From the perspective of using the geochemical data in typical geochemical modeling applications, in a gross sense, there is often little effect on calculated saturation indices among the various filtered waters from the current or previous work. Table 7 lists SI for selected wells (GW-013, GW-040, GW-800) in which the measured turbidity in the current work is much lower than that measured during previous work where three well bore volumes were removed prior to sampling. Regardless of which filter size was used in sampling GW-013, interpretations regarding saturation indices do not vary. The water is undersaturated with respect to all minerals listed in Table 7 for all waters sampled. However, this water contains relatively low contents of colloidal Ca and Ba, and the saturation indices for calcite and barite would not be expected to vary appreciably between the samples because relatively little Ca and Ba are removed from the water through filtration. However, in naturally high turbidity waters in which there is an appreciable percentage of an element which is colloidal, misleading conclusions can be drawn. For instance, GW-040 shows a difference in the SI for barite between the unfiltered and filtered samples in that the unfiltered sample indicates supersaturation, whereas all of the others indicate slight undersaturation with respect to barite. This is to be expected because >50% of the Ba in this well in the larger size fractions is colloidal and is, hence, removed through filtration.

The geochemical modeling results were also used to identify the likely phase of colloidal constituents in the various waters. SI values are reported in Tables 8 and 9, along with the concentration of colloidal (>5 nm) cations in the mineral and the fraction of the cation that is colloidal. The wells with limited colloidal data due to analytical and other uncertainties (the lack of Al data being particularly problematic), or evidence of only a small amount of colloids being present in the water, were omitted from Tables 8 and 9 because any interpretations would be tenuous (GW-058, GW-225, GW-013, GW-074). The reliability of the data was verified by comparing the SI for unfiltered and colloid-free water, assuming that if the colloid is removed by filtration, then the <5-nm SI must be lower than the SI of the unfiltered water for the mineral of interest. These minerals were selected based on minerals previously listed and known to occur in the lithologies.

The likely colloids in GW-684 based on data in Table 8 are evaluated by way of an example. Large changes in the SI of illite, kaolinite, and smectite occur between the unfiltered and <5-nm samples, and all values are supersaturated indicating these colloidal phases may be present in the water. This sample contains appreciable K, Na, Al, and Si colloids indicating that one, or all three, of these minerals may occur as chemically-stable colloids in this water. Part of the colloidal Ca may be contained in calcite as the <5-nm calcite SI is less than the SI calculated using the analysis of unfiltered water. A similar argument can be made in the case of dolomite. Consistent undersaturation with respect to gypsum indicates gypsum is not a likely colloidal phase in this particular water. In addition, quartz is a likely colloid in this water, and minor amounts of barite could be forming the colloids, or Ba could be an impurity in a layered silicate, or be co-precipitating with the calcite. Hence, based on the data in Tables 8 and 9, geochemical modeling with SOLMINEQ indicates that the following colloids are likely stable in the GW-684 water: calcite, dolomite, illite, kaolinite, smectite, quartz, and possibly minor barite.

A similar rationale can be used to identify possible colloidal phases in the other waters. Table 10 summarizes this information for wells in which the colloidal phases were determined using XRD and SEM/EDX. Results from a second type of model are also represented in this table. BALANCE (Parkhurst et al., 1982) was used assuming the unfiltered and filtered waters are analogous to an initial (i.e. unfiltered) and final water (i.e. <5 nm filtered) along a flow path during which precipitation of mineral phases occurred (i.e. colloids). Any mineral phases predicted to precipitate between the unfiltered and filtered waters are minerals assumed to be colloidal. In the BALANCE models, only the following elements and minerals were considered: Ca, Na, K, Si, Al, Fe, Mg, total inorganic carbon, calcite, dolomite, quartz, illite, kaolinite, smectite, chlorite and hematite.

Table 10
Colloidal mineral phases observed with SEM and predicted based on geochemical modeling

		GW-040	GW-061	GW-069	GW-080	GW-095	GW-125	GW-162	GW-684
Calcite	Observed					Y			Y
	Predicted 1			minor		Y	Y	Y	Y
	Predicted 2	Y	Y			Y	Y	Y	Y
Chlorite	Observed		Y				Y	possible	
	Predicted 1						Y?		
	Predicted 2	Y	Y			Y	Y	minor	Y
Clay[a]	Observed	Y			Y	Y	possible	possible	
	Predicted 1		Y		Y	Y			Y
	Predicted 2	Y	Y	minor		Y		Y	Y
Dolomite	Observed								Y
	Predicted 1					Y	Y		Y
	Predicted 2			Y	Y				
Fe-oxide	Observed	Y			Y				
	Predicted 1				Y				
	Predicted 2	Y	Y		Y	Y	Y		
Kaolinite	Observed		Y?						
	Predicted 1	Y			Y	Y			Y
	Predicted 2	Y	Y			Y	Y	Y	
Quartz	Observed		Y		Y			trace	trace
	Predicted 1	Y		Y	Y	Y	Y?	Y	Y
	Predicted 2	Y	Y			Y	Y	Y	Y
Smectite	Observed			Y					
	Predicted 1	Y		Y?	Y	Y			Y
	Predicted 2			Y	Y	Y			Y

Predicted 1: a 'Y' indicates that evaluation of SOLMINEQ results suggest the presence of this colloidal phase.
Predicted 2: a 'Y' indicates that BALANCE results suggest the presence of this colloidal phase.
[a] Clay not identified by SEM and is assumed to be illite where 'Y' indicates a clay colloid is predicted to be present in BALANCE or SOLMINEQ. However, the clay could also be kaolinite or smectite.

In Table 10, mineral phases observed with SEM/EDX and XRD, and those predicted based on SOLMINEQ (Predicted 1) or BALANCE (Predicted 2) results for filtered and unfiltered waters are listed for eight mineral phases identified in seven wells. A 'Y' indicates that the phase was either observed or predicted using one of the two geochemical models. In all cases, when a mineral phase was identified by observation, it was also predicted by at least one of the geochemical models, with the BALANCE results generally being more reliable. However, also note that it is common that mineral phases are also predicted with the geochemical models even though they were not observed as colloids. Hence, the predictive ability of these models is limited because they predict a greater number of colloidal mineral phases than are actually present.

In some cases (e.g. GW-080), an unidentified clay was observed with SEM, and the models predict the presence of illite, kaolinite and smectite. Hence, it is difficult to resolve which clay may be present with the modeling results. Other areas in which the model results are ambiguous are seen in the GW-684 results. The BALANCE model properly predicted the presence of colloidal quartz and calcite, yet it did not predict that dolomite was also a colloidal phase.

Instead, it predicted that smectite was present, likely because the Mg was allocated to the smectite rather than dolomite. Nevertheless, although more phases were predicted than were present, BALANCE predicted most colloidal phases present. In using geochemical models to predict likely colloidal mineral phases present, it must be recognized that it is unlikely that all predicted phases will actually be present in the natural water.

4.4. Variations along hydrologic gradient

Recharge to the Maynardville Limestone wells in the valley floor is from both the Copper Ridge Dolomite and Nolichucky Shale, and these flow paths are reflected in the composition of the colloids. For example, as discussed earlier, wells located in the valley floor receive recharge from the Copper Ridge Dolomite and Nolichucky Shale. One well (GW-725) contains high colloidal Mg (5 mg/l, 26.3% of all Mg) reflecting possible contributions from the Copper Ridge Dolomite, and high Ca (23.1% of all Ca) contributed from both the Maynardville Limestone and Copper Ridge Dolomite, as well high Si (21.2%), K (26.9%) and Na (21.1%) in the larger size fractions expected to be derived from shales.

Fig. 4 shows measured turbidity, total colloidal Ca and Na concentrations, and percentage of the element which is colloidal as a function of flow along an axis parallel to strike from east to west in Bear Creek Valley. No clear trends in these measurements are evident from the data in the Maynardville Limestone wells. No consistently increasing or decreasing trend in the parameters occurs along hydraulic gradient, or with increasing depth. One well (GW-725) completed near the top of the Nolichucky Shale has higher contents of colloidal Na than most of the Maynardville Limestone wells, suggesting possible mixing with water from the Nolichucky Shale. The along-strike flow within the Maynardville Limestone is complicated by the presence of numerous cavities and fractures likely resulting in discrete flow paths to different well locations. Hence, direct comparisons along the general strike-parallel flow path can not easily be made.

Fig. 3 is a cross-section from north to south showing total colloidal concentrations of Na and Ca in wells in the Copper Ridge Dolomite, Maynardville Limestone, Nolichucky Shale, and Pumpkin Valley Shale. GW-040 (Pumpkin Valley Shale) has no colloidal Na, yet high turbidity, likely because the shallower waters in shales have insufficient residence times in the shales to acquire the colloidal Na signature seen in the deeper wells (e.g. GW-117) sampling older waters. The very high turbidity in GW-040 can be attributed to high concentrations of colloidal Al, Fe, and Si, all present in abundance in the shales and overlying weathered soils. The shallow Maynardville Limestone well (GW-058) is a very dilute water containing very low contents of all colloidal material. The deeper Maynardville Limestone wells, on the other hand, show that some of the groundwater from the Nolichucky Shale has likely mixed with water in the Maynardville Limestone (GW-684, 16.7% of the Na is colloidal in the >0.1-μm sizes). The Nolichucky Shale well (GW-117) has very high colloidal Na concentrations, and minimal Ca concentrations, although the colloidal Ca constitutes a large percentage of the total Ca in this water.

In this study, no colloidal Na was detected in any of the lithologies at depths <15 m. In the shales, groundwater evolves from a Ca-Mg-HCO_3 water in shallow recharge areas to a high pH (>9) Na-HCO_3 water along the flow path. Based on field observations and geochemical modeling (Toran and Saunders, 1992), these waters are believed to be produced by alteration of aluminosilicates (dissolution of albite and dolomite) and precipitation of secondary minerals (e.g. kaolinite, smectite and calcite) along short (<1 km) flow paths. Mineralogy plays the major role in the formation of the Na-HCO_3 waters (Toran and Saunders, 1992), and hence these waters are rare in the karstic dolomites and limestones. The fact that there were no observed Na colloids in any formation at shallow depths is, thus, not surprising given the relatively low concentrations of aqueous Na, even in recharge areas of the shales on Pine Ridge. That there are Na colloids in some of the deeper shale wells is reasonable given that smectite is believed to precipitate at the greater depths (Toran and Saunders, 1992). Precipitation of smectite probably occurs in both the immobile and potentially mobile colloidal phase, and smectite colloids were observed in the GW-069 Nolichucky Shale well at a depth of $\approx$ 29 m.

Two shallow Maynardville Limestone groundwaters (GW-058, GW-061) are very dilute, containing

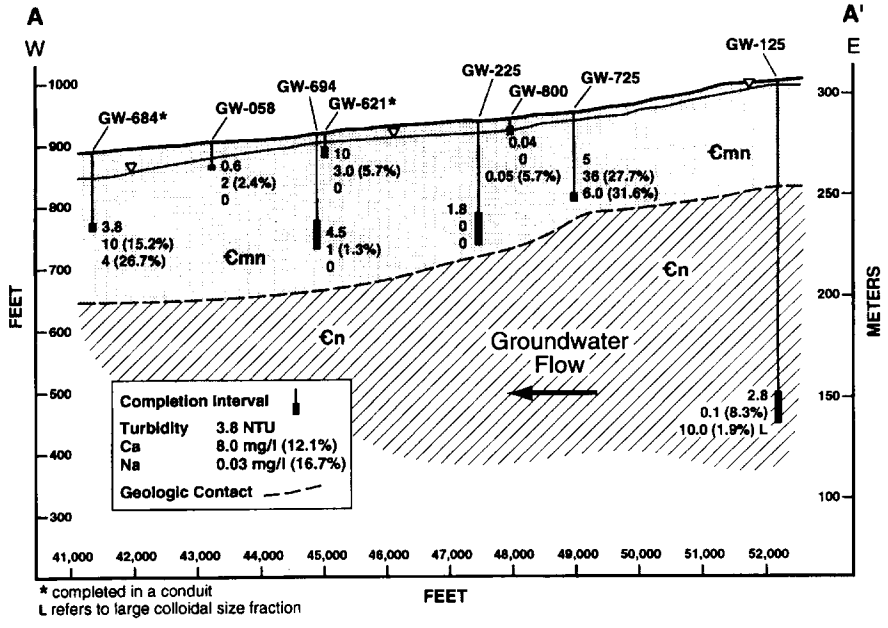

Fig. 4. Along strike cross-section showing measured turbidity, concentration and percentage total colloidal (all size fractions) Ca, and concentration and percentage colloidal Na for seven wells in this study. The location of this cross-section is noted in Fig. 1. No clear trends in these measurements are evident from the data in the Maynardville Limestone wells. No consistently increasing or decreasing trend in the parameters occurs along hydraulic gradient, or with increasing depth. The along-strike flow within the Maynardville Limestone is complicated by the presence of numerous cavities and fractures likely resulting in discrete flow paths to different well locations.

very low contents of all colloidal material (Table 8 Table 9). No colloidal Na occurs in the wells. The deeper Maynardville Limestone wells, on the other hand, show relatively high contents of colloidal Na (GW-684, 26.7% of the Na is colloidal, 4 mg/l). Because colloidal Na is not found in shallower intervals in any lithology, it might be useful as a tracer, though reactive. Groundwater flows from the shales toward the Maynardville Limestone at all elevations (shallow and deeper). Shallow flow to the Maynardville Limestone from shales contains no colloidal Na, and none would be expected in the shallow Maynardville Limestone intervals due to the considerably lower source of Na in this unit. However, the deeper Maynardville Limestone wells contain colloidal Na, which may have arisen from either mixing of some of the groundwater from the Nolichucky Shale with water in the Maynardville Limestone, or by transport of some colloidal-Na between lithologies

Although the chemical composition of the colloids appears to reflect the changes in the chemical composition of waters along the hydrologic gradient, is this evidence that colloids originating in one formation were transported to another formation? That is, are colloids originating in the Nolichucky Shale actually transported to the Maynardville Limestone, or is the Nolichucky Shale contributing water to the Maynardville Limestone that caused saturation and formation of the Na-colloids within the Maynardville Limestone? Thus, the source of the Na colloidal material in the deeper Maynardville Limestone wells (i.e. GW-684) is relevant in assessing possible colloid transport between formations. Based on the mineralogy of colloids and the modeling results, it will be shown that transport of colloids between the Nolichucky Shale and Maynardville Limestone does not appear likely.

A simple mixing model was constructed using BALANCE (Parkhurst et al., 1982) in an attempt to address the issue of colloid transport between these units. GW-061 was selected as the shallow, unmixed Maynardville Limestone end-member. GW-069 was selected as the intermediate depth (29 m) Na-HCO3 end-member fluid in the Nolichucky Shale and is a

less evolved Na-HCO_3 fluid than deeper Nolichucky Shale wells. GW-684 (36.6 m) was selected as the final mixed water in the Maynardville Limestone (Fig. 1). Both dissolved (<5 nm) and total (unfiltered) analyses were used for each of the wells in the models. In order to obtain a water similar to GW-684 from mixing a GW-069 Nolichucky Shale water and shallow Maynardville Limestone water (GW-061), 70% of the mixture would be comprised of the shallow Maynardville Limestone water if analyses of unfiltered water are used, and 76% of the mixture would be comprised of shallow Maynardville Limestone water if <5 nm analyses are used. As a result of mixing the unfiltered waters under equilibrium conditions, and assuming all colloidal and dissolved material are available for reaction, the model predicts calcite, minor gypsum, illite, kaolinite, hematite and dolomite would be dissolved, and smectite and quartz would be precipitated. If colloids are not allowed to react (i.e. if predictions are based on analyses of the <5-nm waters), results are similar except that minor quartz is dissolved, instead of precipitating. In either case, precipitation and dissolution reactions during the mixing of the two waters appear to be important in evaluating the potential for colloidal transport. For example, quartz colloids were observed in both the shallow (GW-061) and deeper (GW-684) Maynardville Limestone fluids and colloidal transport of quartz along strike in the Maynardville Limestone is likely. It is possible that additional colloidal quartz formed during downgradient flow as exemplified by the wells GW-061 and GW-684, and the SOLMINEQ results (Table 8) also support this as the likely case. The SOLMINEQ SI between unfiltered and filtered GW-684 waters decreased measurably, whereas those of GW-061 did not, predicting greater amounts of colloidal quartz in GW-684. Likewise, the BALANCE modeling results are consistent with the presence of calcite and dolomite colloids in the mixed waters. In this model, calcite and dolomite are predicted to dissolve during the mixing of Nolichucky Shale and Maynardville Limestone water, but it is likely that calcite and dolomite colloids form in the Maynardville Limestone after mixing occurs. The mixing results in dissolution which ultimately causes supersaturation of calcite and dolomite and precipitation of apparently mobile colloidal phases within the Maynardville Limestone.

Transport of colloids between the Nolichucky Shale and Maynardville Limestone does not appear likely. Both the Nolichucky Shale (GW-069) and the deeper Maynardville Limestone (GW-684) wells contain colloidal-Na (Table 6). Smectite is predicted by BALANCE to precipitate out of solution in both wells, and the colloidal-Na in the Nolichucky Shale water is likely associated with the observed colloidal smectite structure. However, no colloidal smectite was observed in the mixed GW-684 water (based on analysis of material collected on 0.1-μm filters by XRD and SEM/EDX). The apparent absence of colloidal smectite indicates that these colloids are not only not transported across lithologies from the Nolichucky Shale into the Maynardville Limestone, but that any smectite formed within the Maynardville Limestone when mixing occurs is removed from solution by aggregation (forming large particles that settle) or by electrostatic attachment to surfaces of the formation. The colloidal-Na observed in GW-684 may have co-precipitated out of solution with the quartz, calcite or dolomite colloids during the mixing process. Hence, direct transport of Na-bearing colloids, or other colloids, from the Nolichucky Shale to the Maynardville Limestone is not indicated based on the interpretations made from the geochemical modeling results, and colloids appear to be formed in-situ as a result of mixing of two different groundwaters.

4.5. Chemical and hydrogeologic controls of colloid abundance

Both chemical and hydrogeochemical factors may affect the presence and abundance of colloids in groundwater. To be present in the mobile groundwater phase, suspended colloidal material must be stable [i.e. resistant to either dissolution (chemical stability) or aggregation with other particles (colloidal stability)], and must avoid filtration (i.e. avoid being physically trapped by the immobile aquifer media). Furthermore, colloids already present in the parent geologic material can be released to the groundwater as a result of geochemical or hydrologic processes. Whether a colloid will be stable, aggregated, filtered, settled or resuspended in groundwater depends on a complex combination of surface chemistry, water chemistry and water flow rates.

The colloidal stability and chemical filtration of particles is determined by the balance of repulsive and attractive forces that interact when particles approach one another or approach immobile aquifer surfaces. These interactions have been evaluated quantitatively by the theory of Derjaguin and Landau (1941) and Verwey and Overbeek (1948), known as DLVO theory. Colloidal particles are stabilized when their electric double layers (Lyklema, 1978) are expanded by decreasing electrolyte concentration and ionic strength. The converse promotes particle coagulation or collection of particles on aquifer surfaces. Counterion valence controls double-layer thickness and multivalent cations promote coagulation and collection at much lower aqueous concentrations than do monovalent ions (the Schultze-Hardy rule). Thus, if the presence of colloids in groundwater at the Y-12 site is controlled principally by the colloidal stability of groundwater particles, there should be a strong correlation between the colloid abundance and the ionic strength of the groundwater, and particularly with the concentration of divalent cations (Ca and Mg) compared to monovalent cations (Na and K). Degueldre (1994), who sampled colloids in a number of fractured crystalline formations in Switzerland and Germany, found that this theoretically predicted correlation was observed for natural colloids in these deep, geochemically stable ground waters.

However, physical forces driven by hydrologic processes may also promote the release of attached colloids in fractured or porous media, or may suspend fine particles that settled in cavities in the karst aquifer. Colloid mobilization by physical perturbations can occur if hydrodynamic shear forces, such as an increase in the groundwater flow rate, exceed the adhesive force binding the particle to the surface, as described in DLVO theory, and lift the particle. Large particles will be subjected to much greater drag forces than smaller particles and will be mobilized more easily (Ryan and Elimelech, 1996 and references therein).

Groundwater flow in fractured media may produce velocities capable of causing colloid mobilization. Degueldre et al. (1989), for example, suggested that hydrodynamic shear accounted for the abundance of larger colloids observed in groundwater in fractures in a granite formation in the Swiss Alps. In the shallow groundwater system examined in the current study, storm-driven recharge can lead to rapid changes in water level and presumably in the groundwater flow rate (Shevenell, 1996). Rapid changes in piezometric head have been observed in numerous wells in Bear Creek Valley, especially in the Maynardville Limestone.

The results of the current study show that colloid abundance in groundwater in the Bear Creek Valley is controlled by both chemical factors affecting colloidal stability, as well as hydrologic factors dominated by storm-driven recharge or more rapid flow in conduits and fractures. The observed turbidity is plotted as a function of the concentration of mono- and divalent cations in Fig. 5. If chemical processes controlling colloidal stability dominated, the highest turbidity would be observed at low ionic strength, and turbidity would decrease as the total ionic strength, especially that attributable to divalent cations, increased. For the majority of ground waters, this general relationship is observed. High turbidity was observed in the shallow wells in the water table aquifers. GW-040 and -080 are located near sources of recharge at the top of the ridge and have very low ionic strength. The other water table aquifer wells further from the recharge areas have higher cation concentrations and much lower turbidity. In general, the wells in the karst or fractured aquifer below the water table interval tend to have relatively high ionic strength dominated by divalent cations, and correspondingly low turbidity.

Two wells in the shale aquitard have anomalously high turbidity based on these electrostatic considerations (GW-117 and -125, shown in the back left corner of Fig. 5). Both these wells are deep (>150 m) and in a region that is influenced by mixing with deep brines upwelling beneath the area (Nativ, 1994, 1996), adding significant Na and Cl to the waters (Tables 2 and 3). The elevated turbidity may be real or an artifact. The high pH of the groundwater might have mobilized Fe-oxide colloids in the shales; Fe-containing colloids (probably as Fe-(hydr)oxide) in these wells (Table 6) would likely have a strong negative charge at pH 9 that could lead to repulsive interactions and release of colloids from the formation. Alternately, the change in pressure ($\approx$ 1378–1654 kPa) during sample recovery may cause precipitation of colloidal artifacts. Using SOLMINEQ and the chemistry of unfiltered water in GW-125, some minerals (calcite, dolomite, siderite) could become more saturated as pressure

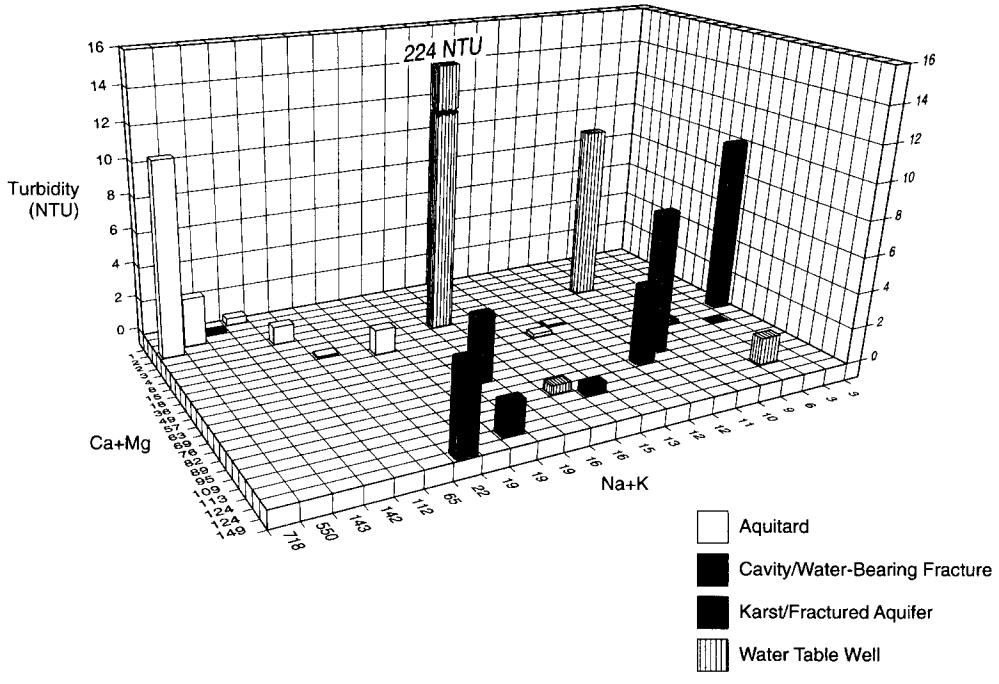

Fig. 5. Relationship between turbidity and the aqueous concentration of mono- and divalent cations. Note that distances along the *x*- and *y*-axes are not proportional to the concentration of ions. Grid lines reflect combinations of mono- and divalent cations observed in individual wells, and thus make it possible to observe the relationship between turbidity and water chemistry for each well.

decreased, but the change in the calculated SI is very small (<1%), and precipitation of these minerals is likely to alter the turbidity by only a minor amount. We cannot discount the possibility that the high turbidity is a sampling artifact caused by infiltration of oxygen into the sampling tubing during the long travel time to the surface, leading to oxidation of dissolved Fe(II) to form Fe-oxide colloids. These uncertainties demonstrate that sampling of such deep wells, even when precautions are taken to prevent hydrologic stress to the aquifer, may be problematic.

There remain five wells that have high turbidities in groundwater with elevated Ca^{2+} concentrations and neutral pH, a combination that is inconsistent with theoretical predictions of colloidal stability. However, all these wells are known to be completed in cavities or water-bearing fractures (Table 1). This indicates that a non-chemical mechanism, probably related to physical mobilization of colloids in zones of high groundwater flow velocities, is also important to account for the observed abundance of colloids. To test this hypothesis, changes in turbidity were monitored in a well during storm events to determine if the piezometric pressure response to recharge was correlated with mobilization of colloids.

4.6. *Effect of storm events on colloid mobilization*

Well GW-621, was monitored during four precipitation events between 8 and 22 May 1995 (Fig. 6). A precipitation event is defined as one continuous period over which rain was measured. This well is completed in cavities in the Maynardville Limestone and is known to undergo rapid changes in water level following recharge events. Although clear increases in turbidity occurred during each of the storms, maximum increases are very small. The highest value was obtained after the first storm. This was the largest storm (5.54 cm over 5.08 h), and although a pre-storm turbidity value was not measured, the peak of 3.95 NTU was the highest seen for the four storms monitored. It is not known whether the increased turbidity results from changes in aqueous

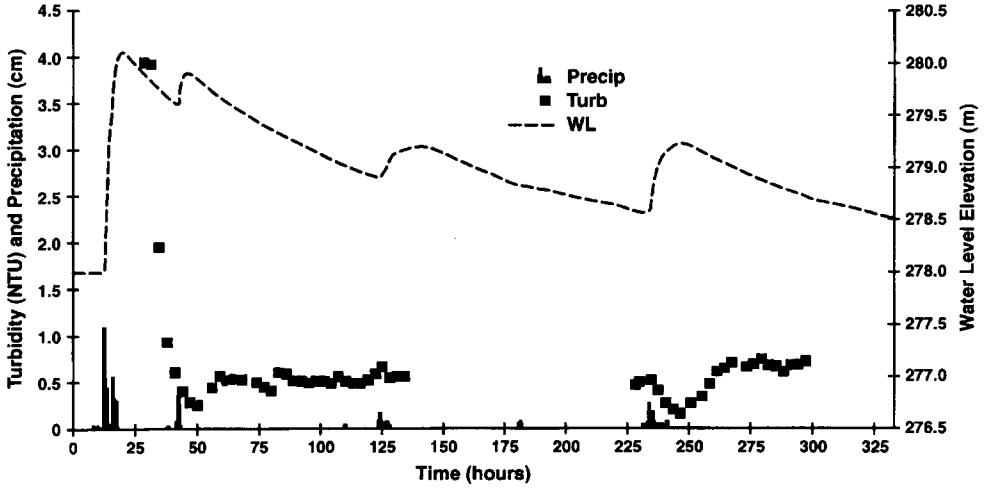

Fig. 6. Water level, precipitation and turbidity in GW-621 during four storm events.

chemistry from infiltrating storm water, or is the result of hydrodynamic forces associated with increased flow velocity in the cavities. These processes are currently being evaluated. Preliminary observations using a colloidal borescope (Kearl et al., 1992) reveal that the colloids mobilized during the storm event are larger in size than the background population, which is consistent with the greater effect hydrodynamic drag forces have on mobilization of larger particles.

5. Summary and conclusions

Groundwater was sampled from a number of wells in fractured shale and karst formations to evaluate the chemical and hydrologic mechanisms controlling the nature and abundance of groundwater colloids. The samples produced by the low-flow methods appeared to be representative of the mobile water and colloids in the groundwater. Not only was the turbidity low, but the colloids that were present were geologically reasonable, reflecting a composition and abundance consistent with lithology, flow paths, and effects of hydrology and aqueous chemistry on colloid mobilization and stability. In general, the larger-size colloids were more abundant in the karstic lithologies, and Ca-containing colloids were more important in the karstic rock, while Na-containing colloids were more important in the shale. The composition of the colloids reflected recharge pathways from the ridges into the Maynardville Limestone in the valley floor. The Mg-colloids in the Maynardville Limestone reflect the possible contributions from the dolomite and the Na, K, and Si in the Maynardville Limestone colloids reflects possible contributions from the shale. There were, however, no clear trends that could be discerned in wells along possible flow paths in the Maynardville Limestone, likely due to the presence of numerous cavities that result in discrete flow paths to different wells. Furthermore, it was not possible to use the colloid composition as a signature to demonstrate colloid transport from one lithology to another. Mixing of Nolichucky Shale and Maynardville Limestone waters and precipitation/dissolution reactions could account for the colloids present in the Maynardville Limestone without invoking transport of specific Nolichucky Shale colloids into the Maynardville Limestone.

The abundance of colloids in groundwater appears to be controlled by both chemical factors affecting colloid stability, as well as physical factors related to hydrology (storm-driven recharge and water velocities). In general, colloids were more abundant in wells with low ionic strength, such as shallow wells in water table aquifers near sources of recharge at the

top of the ridges. Increases in cation concentrations due to dissolution reactions along flow paths were associated with decreases in colloid abundance. However, in spite of elevated ionic strength, colloid concentrations tended to be unexpectedly high in Maynardville Limestone wells that were completed in cavities or water-bearing fractures. The higher levels of colloids appear to be related to higher flow rates in the Maynardville Limestone and storm-driven changes in chemistry that causes resuspension of colloids settled within cavities and fractures.

Our results demonstrate that the potential exists for colloids to have a significant role in contaminant transport, especially in the cavities and fractures in the karst. Although we cannot conclude that colloid-associated contaminants would be transported from the Nolichucky Shale or Copper Ridge Dolomite to the Maynardville Limestone, contaminants in recharge water flowing from the ridges could associate with colloids in the cavities and fractures of the Maynardville Limestone. Storm events appear to be capable of mobilizing this colloidal material. Even though the colloids may not be stable enough in the Ca-rich water to travel long distances before aggregating and settling, repeated re-suspension by storms may move significant loads of colloids—and any associated contaminant—long distances. Understanding of the chemical and physical mechanisms controlling colloid transport during storm events would make it possible to better assess the importance of colloids to long-distance transport in the karst.

Acknowledgements

The authors are indebted to a group of hard-working research technicians who sampled the wells and helped tabulate and analyze the data, including J.A. McDonald, T.L. Knowles, B.T. Sheldon, C.R. Knight and K.F. Smart. We thank J.N. Ryan and C. Rightmire for reviewing an early draft of this manuscript. We thank G. Davies, C.G. Groves and P. Huntoon for their helpful comments and suggestions in review of the manuscript. This research was supported by the Oak Ridge Y-12 Plant (Y-12) Environmental Management Department, Ground Water Protection Program, and the support of W.K. Jago and the assistance of E.B. Rundell, B.W. McMaster and L. Dillon are gratefully acknowledged. Y-12 is managed by Lockheed Martin Energy Systems, Inc. for the US Department of Energy (DOE) under contract DE-AC05-84OR21400. The Oak Ridge National Laboratory (ORNL) is managed by Lockheed Martin Energy Research Corp. for DOE under contract number DE-AC05-96OR22464. Partial support for this work was provided to the second author by Lockheed Martin Energy Systems, Inc. under subcontract 87X-SP923V to the University of Nevada, Reno. Publication No. 4724 of the Environmental Sciences Division, ORNL.

References

Buffle, J., 1988. Complexation Reaction in Aquatic Systems: An Analytical Approach. Ellis Horwood Ltd, Chichester, UK.

Degueldre, C.A., 1994. Colloid Properties in Ground waters from Crystalline Formations. Paul Scherrer Institut, Bericht Nr. 94-21.

Degueldre, C., Baeyens, B., Görlich, W., Riga, J., Verbist, J., Stadelmann, P., 1989. Colloids in water from a subsurface fracture in granitic rock, Grimsel test site, Switzerland, Geochim. Cosmochim. Acta., 53, 603–610.

de Laguna, W.T., Tamura, T., Weeren, H.O., Struxness, E.G., McClain, W.C., Sexton, R.C., 1968. Engineering development of hydraulic fracturing as a method for permanent disposal of radioactive wastes. Oak Ridge National Laboratory Report 4259.

Derjaguin, B.V., Landau, L., 1941. Acta Physicochim. USSR, 14, 633.

Desmarais, K.M., 1995. Carbonate spring response to storm events, Bear Creek Valley, Tennessee. Oak Ridge Y-12 Report Y/TS-1555.

Goldstrand, P., 1995. Stratigraphic variations and secondary porosity within the Maynardville Limestone in Bear Creek Valley, Y-12 Plant. Y-12 Plant Report Y/TS-1093.

Goldstrand, P.M., Shevenell, L.A., 1997. Geologic controls on porosity development in the Maynardville Limestone, Oak Ridge, Tennessee, Environmental Geology, 31 (3/4), 259–269.

Hatcher, R.D., Jr., Lemiszki, P.L., Dreier, R.B., Ketelle, R.H., Lee, R.R., Lietzke, D.A., McMaster, W.M., Foreman, J.L., Lee, S.Y., 1992. Status report on the geology of the Oak Ridge Reservation. Oak Ridge National Laboratory Report ORNL/TM-12074.

HSW Environmental Consultants, Inc., 1993. Ground water quality assessment for the Bear Creek hydrogeologic regime at the Y-12 Plant: 1992 ground water quality data and calculated rate of contaminant migration. Y-12 Plant Report Y/SUB/93-YP507C/1/P1.

Jones S.B., Harrington, B.K., Field, S.M., 1992. Updated subsurface data base for Bear Creek Valley, Chestnut Ridge, and parts

of Bethel Valley on the U.S. Department of Energy Oak Ridge Reservation. Y-12 Plant Report, Y/TS-881.

Kearl, P.M., Korte, N.E., Cronk, T.A., 1992. Suggested modifications to ground water sampling procedures based on observations from the colloidal borescope, Ground Water Monitoring Review, Spring, 155–160.

Kharaka, Y.K., Gunter, W.D., Aggarwal, P.K., Perkins, E.H., DeBraal, J.D., 1988. SOLMINEQ.88: A computer program for geochemical modeling of water–rock interactions. U.S. Geol. Survey Water-Resources Investigations Report 88-4227.

King, H.L., Haase, C.S., 1987. Subsurface-controlled geological maps for the Y-12 Plant and adjacent areas of Bear Creek Valley. Oak Ridge National Laboratory Report ORNL/TM-10112.

Lyklema, J., 1978. Surface chemistry of colloids in connection with stability. In: Ives, K.J. (Ed.), The Scientific Basis of Flocculation. Sijthoff and Noordhoff, Dordrecht, The Netherlands, pp. 3–36.

McCarthy, J.F., Degueldre, C., 1993. Sampling and characterization of ground water colloids for studying their role in the subsurface transport of contaminants. In: Buffle, J., van Leeuwen, H. (Eds.), Environmental Particles, Volume II. Lewis Publishers, Chelsea, MI, Ch. 6, pp. 247–315.

McCarthy, J.F., Shevenell, L., 1998. Sampling colloids in a fractured and karst aquifer. Ground Water, 36, 251–260.

McCarthy, J.F., Zachara, J.M., 1989. Subsurface transport of contaminants: binding to mobile and immobile phases in ground water aquifers, Environ. Sci. Technol., 23, 496–504.

McDowell-Boyer, L.M., Hunt, J.R., Sitar, N., 1986. Particle transport through porous media, Water Resources Research, 22 (13), 1901–1921.

McKay, L.D., Cherry, J.A., Bales, R.C., Yahya, M.T., Gerba, C.P., 1993. A field example of bacteriophage as tracers of fracture flow, Environ. Sci. Technol., 27 (6), 1075–1079.

Nativ, R., 1994. The deep hydrogeologic flow system underlying the Oak Ridge Reservation, Geol. Soc. Am. Abstracts with Programs, 26 (3), 65–66.

Nativ, R., 1996. The brine underlying the Oak Ridge Reservation, Tennesses, USA: characterization, genesis, and environmental implications, Geochemica. Cosmochim. Acta, 60 (5), 787–801.

Parkhurst, D.L., Plummer, L.N., Thorstenson, D.C., 1982. BALANCE—aA computer program for calculating mass transfer for geochemical reactions in ground water. U.S. Geol. Surv. Water-Resources Investig. 82-14.

Ryan, J.N., Elimelech, M., 1996. Colloid mobilzation and transport in ground water. Colloids and Surfaces A: Physocochemical and Engineering Aspects, 107, 1–56.

Saunders, J.A., Toran, L.E., 1994. Evidence for dedolomitization and mixing in Paleozoic carbonates near Oak Ridge, Tennessee, Ground Water, 32 (2), 207–214.

Shevenell, L., 1996. Analysis of well hydrographs in a karst aquifer: Estimates of specific yields and continuum transmissivites. J. Hyd., 174, 331–355.

Shevenell, L.A., 1994. Chemical characteristics of waters in karst formations at the Oak Ridge Y-12 Plant. Y-12 Plant Report Y/TS-1001.

Shevenell, L.A., Beauchamp, J.J., 1994. Evaluation of cavity occurrence in the Maynardville Limestone and the Copper ridge Dolomite at the Y-12 Plant using logistic and general linear models. Y-12 Plant Report Y/TS-1022.

Shevenell, L., Dreier, R.B., Jago, W.K., 1992. Summary of fiscal year 1991 and 1992 construction, hydrologic and geologic data obtained from the Maynardville Limestone Exit Pathway Monitoring Program. Y-12 Plant Report Y/TS-814.

Shevenell, L., Goldstrand, P.M., 1994. Effectiveness evaluation of three RCRA Caps at the Y-12 Plant, Oak Ridge, Tennessee. Y-12 Plant Report Y/TS-891.

Shevenell, L., McMaster, B., Desmarais, K., 1995. Evaluation of cross borehole tests at selected wells in the Maynardville Limestone and Copper Ridge Dolomite at the Oak Ridge Y-12 Plant. Y-12 Plant Report Y/TS-1166.

Shevenell, L., McMaster, B., 1996. Interpretation of well hydrographs in the karstic Maynardville Limestone at the Oak Ridge Y-12 Plant. Y-12 Plant Report Y/SUB/96-SP912V/1.

Shevenell, L.A., Moore, G.K., Dreier, T.B., 1994. Contaminant spread and flushing in fractured rocks near Oak Ridge, Tennessee, Ground Water Monitoring and Remediation, XXIV (2), 120–129.

Toran, L.E., Saunders, J.A., 1992. Geochemical and ground water flow modeling of multiport-instrumented coreholes (GW-131 through GW-135). Oak Ridge Y-12 Report Y/TS-875 (ORNL/GWPO-0004).

USEPA, 1994. Ground water sampling—a workshop summary, U.S. Environmental Protection Agency, Dallas, TX, 30 November–2 December 1993, EPA/600/R-94/205.

Verwey, E.J.W., Overbeek, J.Th.G., 1948. Theory of the stability of lyophobic colloids. Elsevier, Amsterdam.